ANALYZING POROSITY USING PETROGRAPHIC IMAGING METHODS: KEY FOR PETROPHYSICS

An Undergraduate Research Scholars Thesis

by

KATHLEEN MCDANIEL

Submitted to Honors and Undergraduate Research
Texas A&M University
in partial fulfillment of the requirements for the designation as an

UNDERGRADUATE RESEARCH SCHOLAR

Approved by
Research Advisor: Dr. Juan Carlos Laya

May 2014

Major: Geology

TABLE OF CONTENTS

ABSTRACT

Analyzing Porosity using Petrographic Imaging Methods: Key for Petrophysics. (May 2014)

Kathleen McDaniel
Department of Geology and Geophysics
Texas A&M University

Research Advisor: Dr. Juan Carlos Laya
Department of Geology and Geophysics

The porosity in rock can be quantified and characterized using a variety of direct methods including imbibition methods, mercury injection, gas expansion, petrography, X-ray tomography, and image analysis. However many of them can be complex and more expensive than petrographic image analysis. In the oil industry, it is a common practice to use the indirect methods such as well-logs and seismic to identify rock properties like porosity and permeability. However, these methods do not always represent the physical reality and need to be calibrated with direct measurements. For that reason, the main objective of this project is to assess the efficiency and precision of petrographic image analysis to provide useful data for petrophysics studies. In order to face this problem, a database comprised of 400 high-resolution images of thin section slides extracted from carbonate rock samples is classified. Once classified, the samples are subjected to experimental methods of measuring porosity using petrographic imaging software. The results demonstrate the suitability of the methods to provide reliable data for petrophysics studies.

ACKNOWLEDGEMENTS

I would like to thank my research advisor, Dr. Juan Carlos Laya, for providing me with this research opportunity, giving me helpful advice, and supporting the completion of this project.

I would also like to thank Sandra Tonietto for working one-on-one with me as we described thin sections and used the image analysis software.

CHAPTER I

INTRODUCTION

The application of image analysis towards solving problems related to the geosciences and petrophysics has been utilized extensively, especially in characterizing reservoir rocks. Pore spaces can be complex in geometry and connectivity; therefore various methods have been developed in an attempt to accurately measure porosity including manual point counting, petrography, and image analysis. When using image analysis, high resolution scans must be used and may require different magnifications for improved precision, providing ample data on pore shapes and distribution throughout the rock sample. This can give information on certain surface measurements, "the interstitial surface area of the pores per unit of bulk volume of porous material," and provide estimations on permeability since "permeability tends to increase as porosity increases and specific surface decreases" (Ruzyla 1986). Advances in image analysis have made the process more efficient and timely by adding such features as segmentation in detecting pigmented epoxy in pore spaces so digital filters will analyze the pores instead of the entire rock (Ehrlich et al. 1984). In his thesis on determining the effectiveness of imaging analysis on characterizing reservoirs, Layman (2002) found that the method allows for the quick and dependable reconstruction of reservoir pore facies when compared to the manual inspection of thin sections.

Location of Dickinson Field

The thin sections utilized for the study of petrographic and petrophysical correlations are taken from cores drilled in Dickinson Field, North Dakota along the south-central section of Williston

Basin. The field is located in the southwestern part of North Dakota in northern Stark County (Figure 1) and the cores were taken from two of the oil-producing fields in the Dickinson region (Figure 2). The Steffan 1-35 core is from a well drilled in Duck Creek field and the Steffan 2-2 core is from a well drilled in Eland field (Adams 1999).

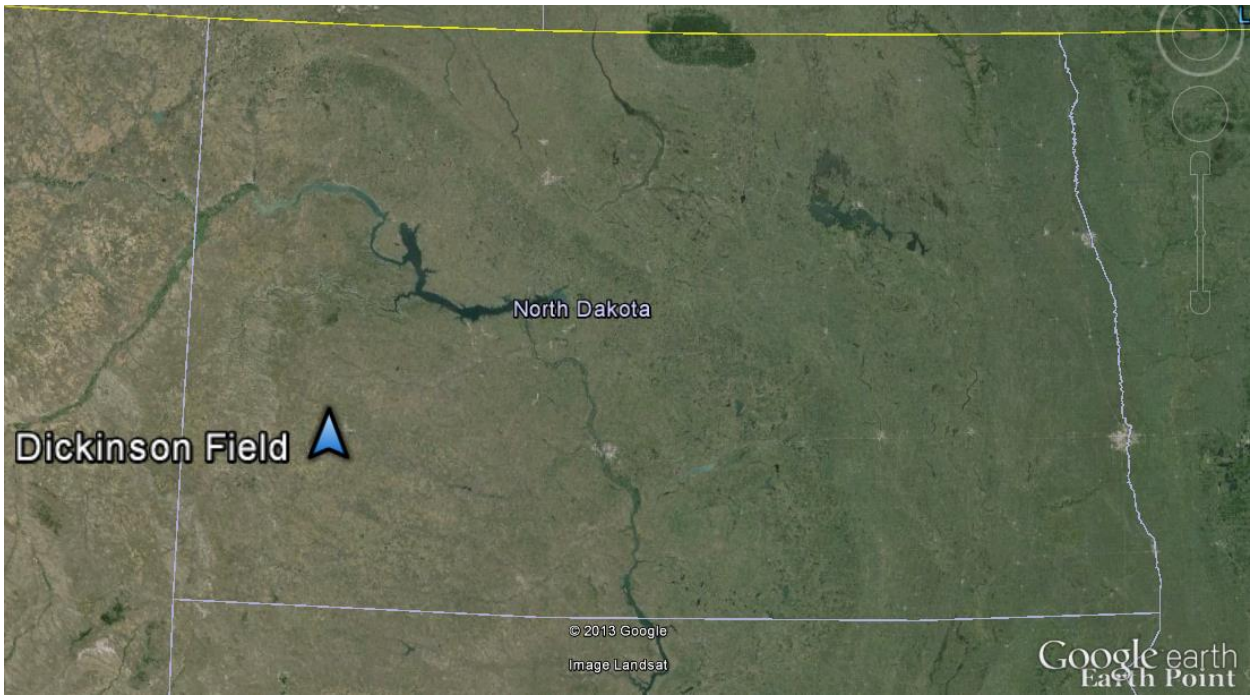

Figure 1. Dickinson Field, North Dakota at 47°07’09.61” N, 102°58’31.79” W (Google Earth)

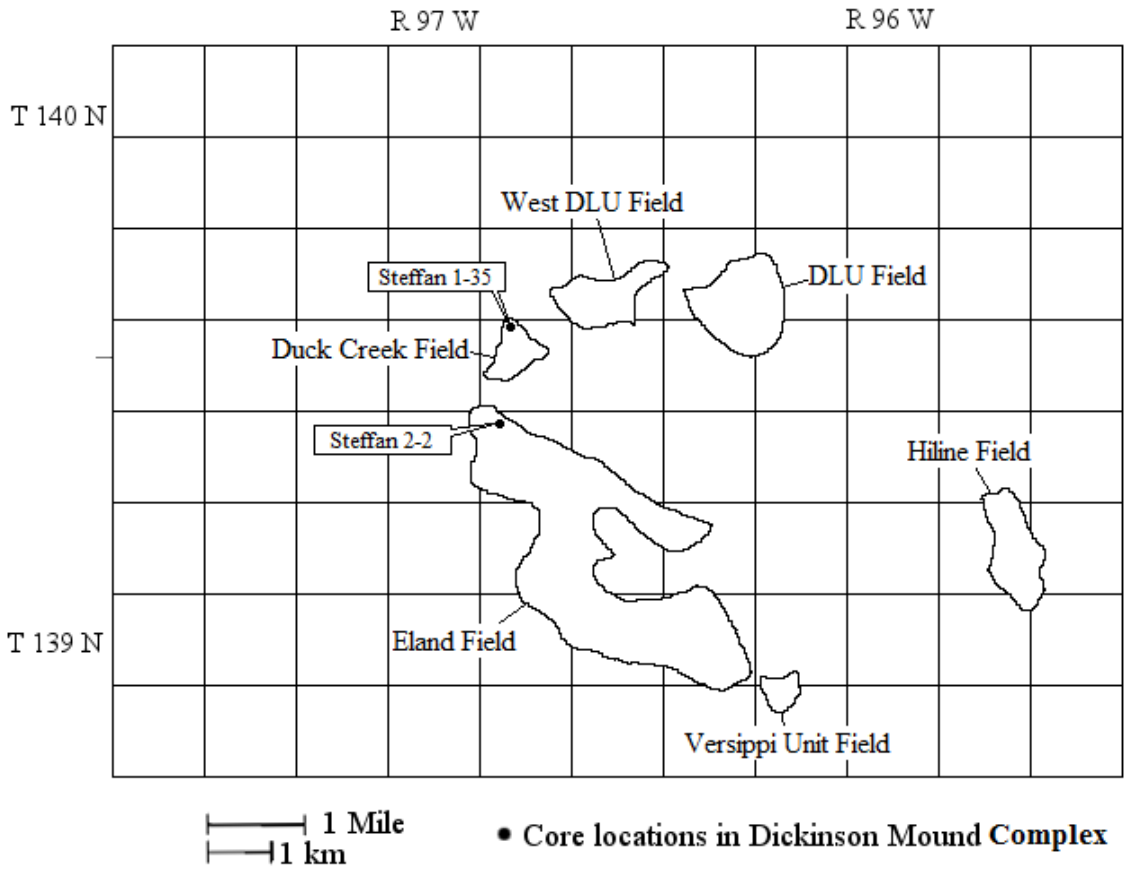

Figure 2. Locations of cores from Steffan 1-35 and Steffan 2-2 in Dickinson Field (modified after Adams 1999).

Geology of Dickinson Field

The focus of this study in Dickinson Field, North Dakota is on the Mississippian-aged Lodgepole Formation that constitutes part of the Madison Group (Figure 3). During its deposition, this formation gradually experienced maximum flooding with the fluctuating sea level and was populated by diverse marine life during the transgressive-regressive cycle spanning the Madison Group (Adams 1999).

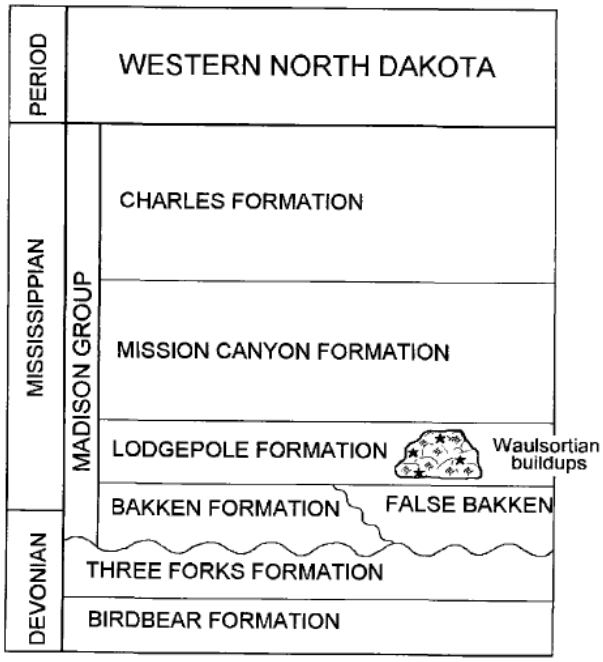

Figure 3. Stratigraphic column of Western North Dakota (Adams 1999).

The Lodgepole Formation almost completely consists of limestones and calcareous shale formed from the deposition of marine organisms and sediments on an oceanic shelf. Dickinson Field is composed of a cluster of mounds trapping oil in the subsurface and these are described as Waulsortian buildups or "carbonate buildups consisting of lime mudstone, wackestone and packstone with limited amounts of grainstone and abundant fossil fragments, mostly bryozoans and crinoids" (Johnson 1995). These carbonate buildups are found in the south-central section of Williston Basin, an intracratonic structure, and this section is dominated by north-south trending structures (Adams 1999).

Core Descriptions

Steffan 1-35

The Steffan 1-35 core, taken from the northern portion of Duck Field, extends from a depth of 10,043 feet to 9,827 feet. From the base trending upwards, the core transitions between various carbonate rock types that contain diverse fossil assemblages. These intervals are summarized below in Table 1. Moundstones describe the carbonate buildups and are primarily made up of mudstone and wackestone. Cementstones describe rock made up of clay- and silt-sized carbonate grains. The first 32 feet contains alternating bioclastic packstones and grainstones with calcareous muds. The next 9 feet is composed of porosity-enhanced, steeply inclined, stylolitic packstone and grainstone. The following 18 feet includes nearly horizontal to slightly inclined bioclastic packstone/grainstone containing scattered moundstone and cementstone with calcareous muds. The subsequent 15 feet is comprised of moundstone/cementstone with fossil-rich wackestone layers and voids filled with mud pockets. The next 44 feet is composed of moundstone/cementstone with slightly to steeply inclined wackestone/packstone interbedded with layers of grainstone and cementstone. The following 33 feet includes moundstone/cementstone with massive, stylolitic wackestone and thin, alternating packstone and grainstone layers. The subsequent 61.5 feet is comprised of alternating moundstone-cementstone and detrital packstone-grainstone units. The final 34.5 feet is composed of massive moundstone and cementstone (Adams 1999).

Table 1. Summary of 1-35 Core Description (modified from Adams 1999)

Well Name	Cored Interval (depth in feet)	Unit Thickness (feet)	Lithology *	Sedimentary Features †
1-35	9,827	35	G	Massive, detrital material, diverse fragmented fossils
	9,829	1	MS/CS	Steeply inclined RFC/fenbry sheets, SV with spar, good porosity
	9,848	20	Detrital P/G	High fossil diversity, disarticulated hash
	9,850	2	MS/CS	Steeply inclined, detrital mud pockets, SV, RFC, rim cement
	9,869	18	Detrital G	Diverse biota, intergranular, moldic & enhanced porosity in vugs, HC stain
	9,873	4	Alt W/P/G/CS	Horizontal bedding, low porosity, fewer SV, detrital mud, HC stain
	9,880	5	CS	Fenestrate-rich, small vugs fill w/ BC, SV, enhanced porosity
	9,882	2	P/G	Stylolitic, "spongy" appearance, HC stain, crinoidal hash, hairline frx
	9,888	6	MS/P/G	Massive, SV, stylolitic, open and healed frx, HC stain, enhanced porosity
	9,921	33	MS/CS	SV, highly fractured, detrital mud, stylolites, healed frx, mod. Incline
	9,965	44	MS/CS	Massive, RFC, SV, inclined bedding, detrital mud, enhanced porosity
	9,980	15	MS/CS	Massive, RFC, SV, detrital mud, stylolites, porosity enhanced vugs/frx
	9,998	18	Alt bio P/G	IB W/CS, slightly inclined, detrital mud, Poorly dev. Spar in SV, many frx
	10,007	9	P/G	Steeply inclined, stylolitic, HC stain, SD in B molds
	10,043	32	Alt P/G	3-10 " beds, detrital layers, HC stain, SD in frx

*: W=Wackestone, P=Packstone, G=Grainstone, MS=Moundstone, CS=Cementstone
†: disc=discontinuous, frx=fractures, SD=saddle dolomite, bioturb=bioturbated, dolo=dolomite, SV=stromatactoid vug, C=crinoids, RFC=radiaxial fibrous calcite cement, HC=hydrocarbon, mod=moderate, dev=developed, B=brachiopod, IB=interbedded

Steffan 2-2

The Steffan 2-2 core, taken from the northern portion of Eland Field, extends from a depth of 9,989 feet to 9,949 feet. These intervals are summarized below in Table 2. The first 7.4 feet contains wavy-bedded, inclined, stylolitic wackestone/packstone that is interbedded with mudstone/wackestone. The next 1 foot is composed of a grainstone with layered crinoids. The following 5 feet includes slight to moderately inclined wackestone/packstone and is interbedded with detrital muds. The subsequent 2 feet is comprised of wavy-bedded, discontinuous, stylolitic grainstone. The next 2 feet is composed of wavy- and parallel-bedded grainstone. The following 8.5 feet includes steeply dipping wackestone with stylolites at the top and is interbedded with

mudstone and peloidal packstone/grainstone. The subsequent 6.6 feet forms a sharp contact with the lower unit and is comprised of alternating mudstone and wackestone. The final 7.5 feet is composed of interbedded, steeply inclined, wavy-bedded packstone and grainstone (Adams 1999).

Table 2. Summary of 2-2 Core Description (modified from Adams 1999)

Well Name	Cored Interval (depth in feet)	Unit Thickness (feet)	Lithology *	Sedimentary Features †
2-2	9,949	2	P/G	Steeply inclined, wavy, stained, frx heated with calcite and SD
	9,954	5	P/G	Steeply inclined, wavy, SV, vuggy, SD in frx, dissolution of pores
	9,958	4	Alt M/W	Peloidal, muddy, large frx healed with SD
	9,966	12	W	IB M/P/G, sleep dip, platy, stylolitic, SD in vugs and frx, dissolution
	9,970	2	G	Wavy, parallel, stylolitic, detrital muds, frx healed with SD
	9,973	2	G	Disc, wavy, stylolitic, vuggy, HC stain
	9,980	5	W/P	IB detrital muds, peloidal, clasts, vuggy, SD crystals, healed frx with SD
	9,981	1	G	Detrital, crinoidal, aligned fossils, hydrocarbon residue
	9,989	8	W/P	Inclined, IB M/W, platy/wavy, stylolitic, SD crystals, open/healed frx

*: M=Mudstone, W=Wackestone, P=Packstone, G=Grainstone

†: disc=discontinuous, frx=fractures, SD=saddle dolomite, bioturb=bioturbated, dolo=dolomite, SV=stromatactoid vug, C=crinoids, RFC=radiaxial fibrous calcite cement, HC=hydrocarbon, mod=moderate, dev=developed, B=brachiopod, IB=interbedded

CHAPTER II

METHODS

Thin section examinations were made using image analysis software, Image-Pro Premier, in the laboratory. This software calculates the pore space in an image by receiving different signals from color-coded voids and grains and taking geometric measurements using processes of segmentation and image skeletonization to simplify the three dimensional void space (Lindquist and Venkatarangan 1999). The Texas A&M library resources were used to compare data, investigate different methods of finding porosity, and examine previous research. Once the information was compiled, correlations between rock characteristics and porosity were made. A workflow was established to guide the progression from obtaining the thin sections to qualitatively and quantitatively analyzing them (Figure 4).

Figure 4. Workflow diagram.

Database

The thin section image database contains approximately 300 thin sections with about 400 images of carbonate rock from outcrops and subsurface cores in different areas. The images were scanned by a Nikon Super CoolScan 8000 slide and film scanner at high resolution. Information

in the database includes the company or university that worked on the thin section, general location, field site, well name and number, thin section slide label, depth, formation name, rock type, facies, presence of porosity, presence of blue epoxy, and description of the rock in the thin section. A condensed table of this information is provided in Appendix A. The presence of porosity and blue epoxy is significant since both aid in the efficient calculation of pore space properties in the petrographic image analysis software.

Petrographic Image Analysis

Qualitative Description

Carbonate rocks exhibit high heterogeneity in composition caused by such factors as the depositional environment, fluctuating sea levels, biotic diversity, dissolution and cementation processes, and post-depositional impacts, such as fault movements causing fracturing. These factors alter pore space, modify or destroy previous compositions, and create complex compositional and biological frameworks. Heterogeneity in carbonates makes it difficult to simply evaluate rock and reservoir properties, hindering the efficient discovery and extraction of natural resources in the subsurface. Therefore, three different porosity and petrophysical classifications were developed by Ahr, Choquette and Pray, and Lucia to improve the organization and description of the wide range of carbonates. This additional information is added to the database to catalog visual assessments of the images.

First, the images are listed by Ahr's (2005) carbonate porosity classification system (Figure 5). This classification system categorizes carbonates based on how their porosity was developed and is helpful in understanding how the rock's properties formed. Three different categories -

Depositional, Diagenetic, and Fracture - are displayed to describe the origin of that rock's porosity and any number of hybrid pore types occur between the categories. In Figure 5, "depositional porosity represents space that remains between grains, such as the ooids in the scanning electron micrograph (top), skeletal fragments or other particles. Diagenetic porosity, filled with blue epoxy in a thin section of dolomitized limestone (left), can result from cementation, compaction, dissolution, recrystallization or replacement processes. Fracture porosity can occur at more than one scale, as is shown by at least two fracture sets in the outcrop photograph (bottom right)" (Ahr 2005).

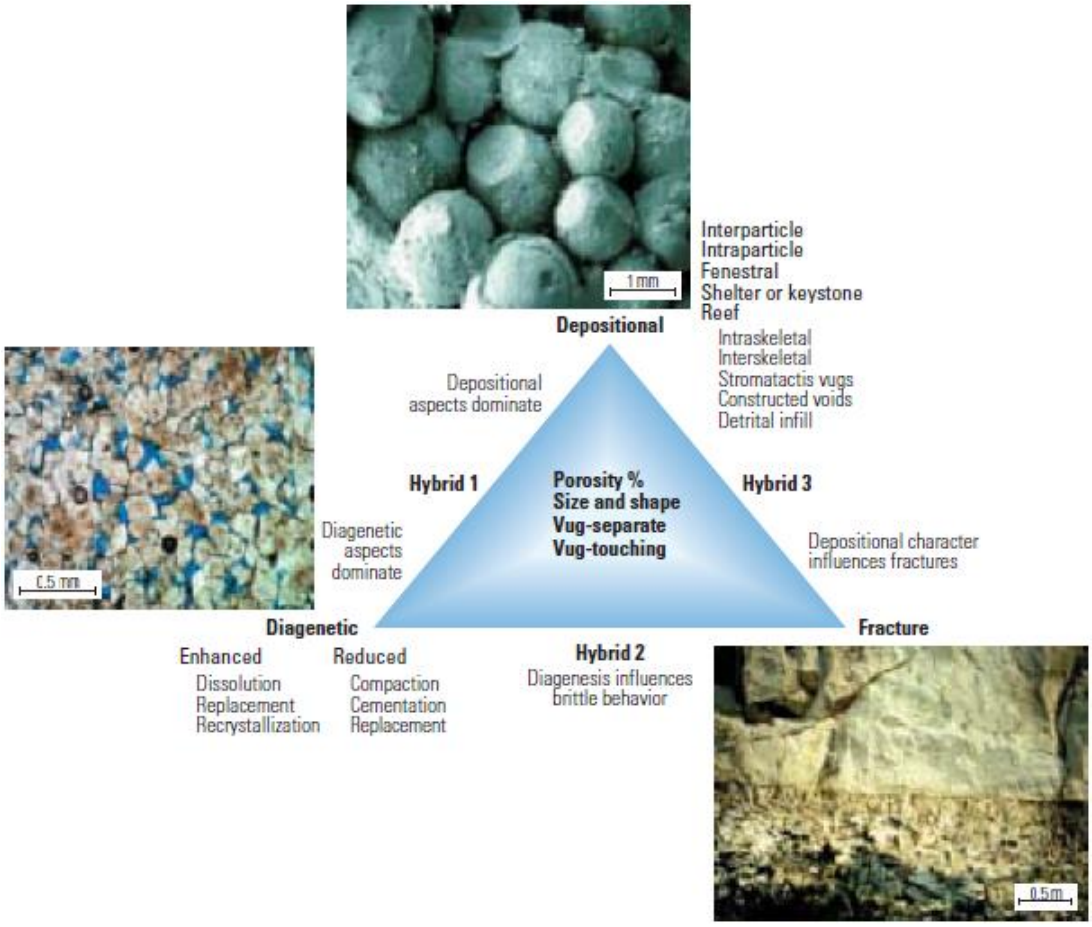

Figure 5. Wayne Ahr's carbonate porosity classification (Photographs of ooids and fractures courtesy of Wayne Ahr; photograph of intercrystalline porosity courtesy of David C. Kopaska-Merkel) (Ahr 2005).

Secondly, the images are listed by Choquette and Pray's (1970) carbonate porosity classification system (Figure 6). This classification system categorizes carbonates based on the presence of specific types of porosity and these types of properties form based upon pore "size, shape, genesis, or position with respect to fabric elements of the rock" (Choquette and Pray 1970). The system narrows down the description of pore space and aids in the determination of what porosity type dominates in the thin sections.

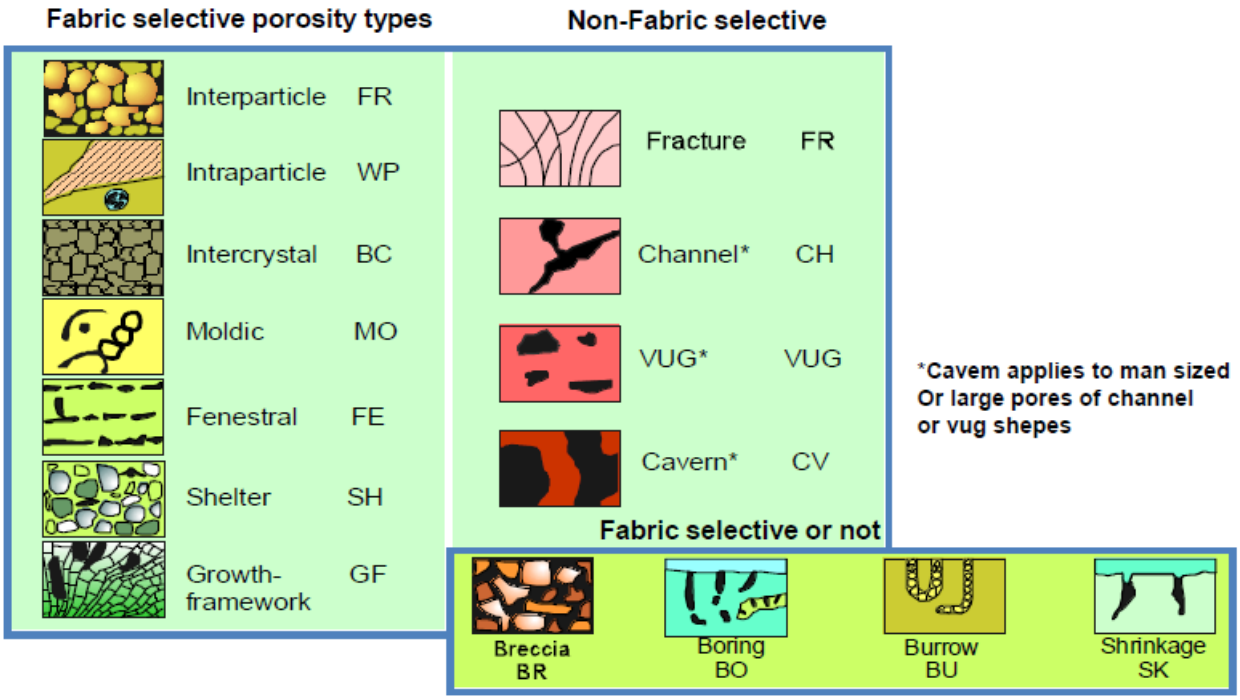

Figure 6. Philip Choquette and Lloyd Pray's carbonate porosity classification (Choquette and FPray 1970).

Thirdly, the images are listed by Lucia's (1995) carbonate porosity classification system that involves characterizing vuggy pore space, interparticle pore space, and petrophysical classes. This classification system categorizes carbonates based on what type of pore space they exhibit and on capillary properties that determine the amount of porosity and connectivity of the pores.

In Figure 7, the vuggy pore space of samples is sorted by mud- or grain-dominated fabric and then the pores are examined to discern what specific types they encompass.

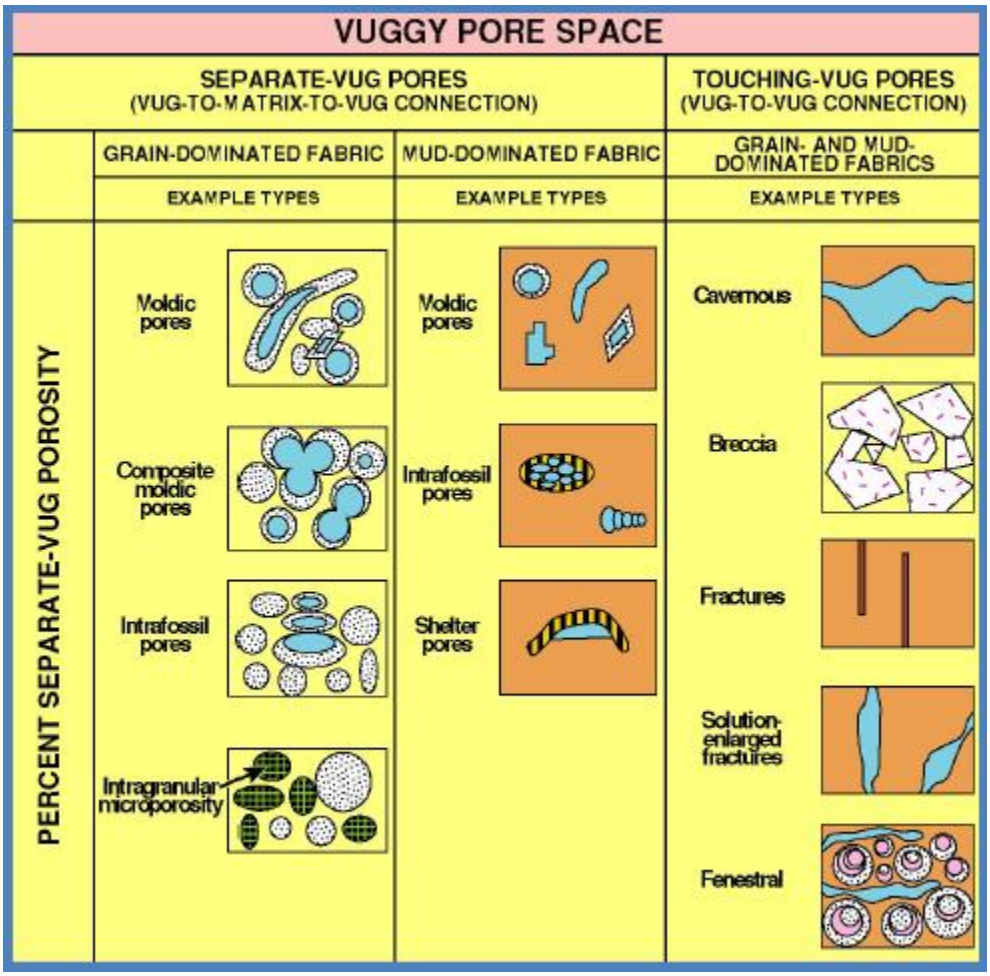

Figure 7. F. Jerry Lucia's classification of vuggy pore space based on vug interconnection (Lucia 1995).

In Figure 8, the samples are grouped by mud- or grain-dominated fabric and specific rock type of mudstone, packstone, wackestone, or grainstone. In Figure 9, Dunham's (1962) classification is also utilized to better clarify these rock types and these classifications quickly display how much mud or grain content there is versus the skeletal grain content.

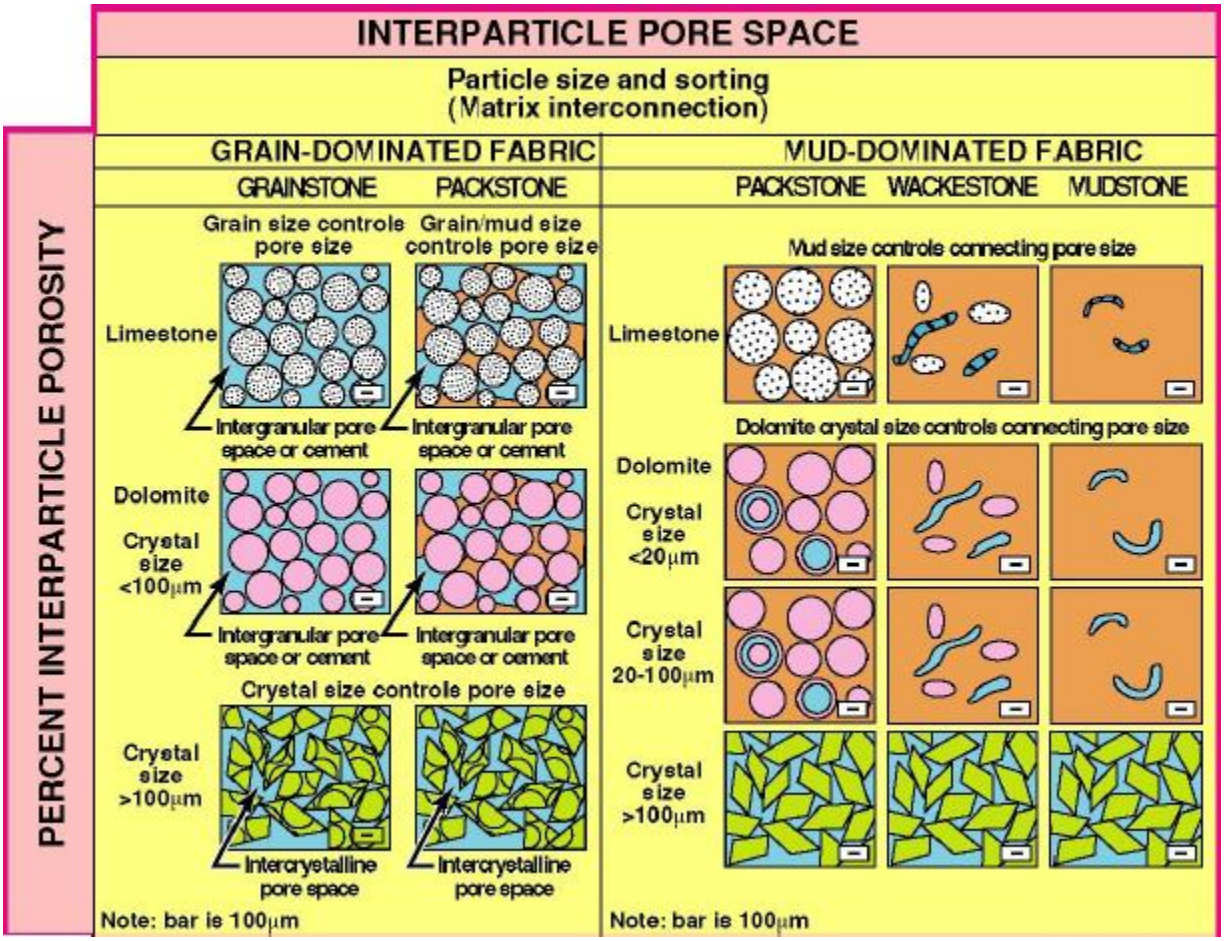

Figure 8. F. Jerry Lucia's classification of carbonate interparticle pore space based on size and sorting of grains and crystals (Lucia 1995).

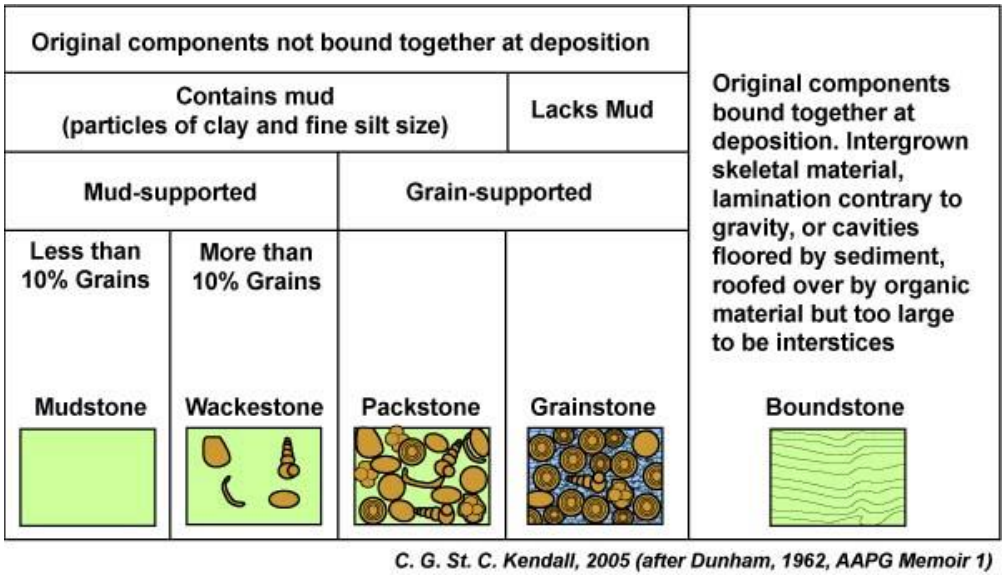

Figure 9. Robert Dunham's classification of carbonate rock based upon mud- or grain-support and skeletal grain content (SEPM 2013).

In Figure 10, the samples are grouped into petrophysical Class 1, 2, or 3 based upon their fabric type and pore space determined by the characterization of the vuggy pore space and interparticle pore space in Figures 7 and 8. However, Lucia only found relationships between porosity and separate-vug pore systems or interparticle space, not between porosity and touching-vug pore systems. Lucia assessed the classes with capillary curves of limestone and dolomite rock fabrics, producing three sets of equations approximating permeability (k) and water saturation (S_w) from interparticle porosity (ϕ_{ip}), fractional porosity (ϕ), and height above capillary pressure equal to zero (H):

Class 1:

$$k = (45.35 \times 10^{8}) \times \phi_{ip}^{8.537} \quad (1)$$

$$S_w = 0.02219 \times H^{-0.316} \times \phi^{-1.745} \quad (2)$$

Class 2:

$$k = (2.040 \times 10^{6}) \times \phi_{ip}^{6.38} \quad (3)$$

$$S_w = 0.1404 \times H^{-0.407} \times \phi^{-1.440} \quad (4)$$

Class 3:

$$k = (2.884 \times 10^{3}) \times \phi_{ip}^{-1.210} \quad (5)$$

$$S_w = 0.6110 \times H^{-0.505} \times \phi^{-1.210} \quad (6)$$

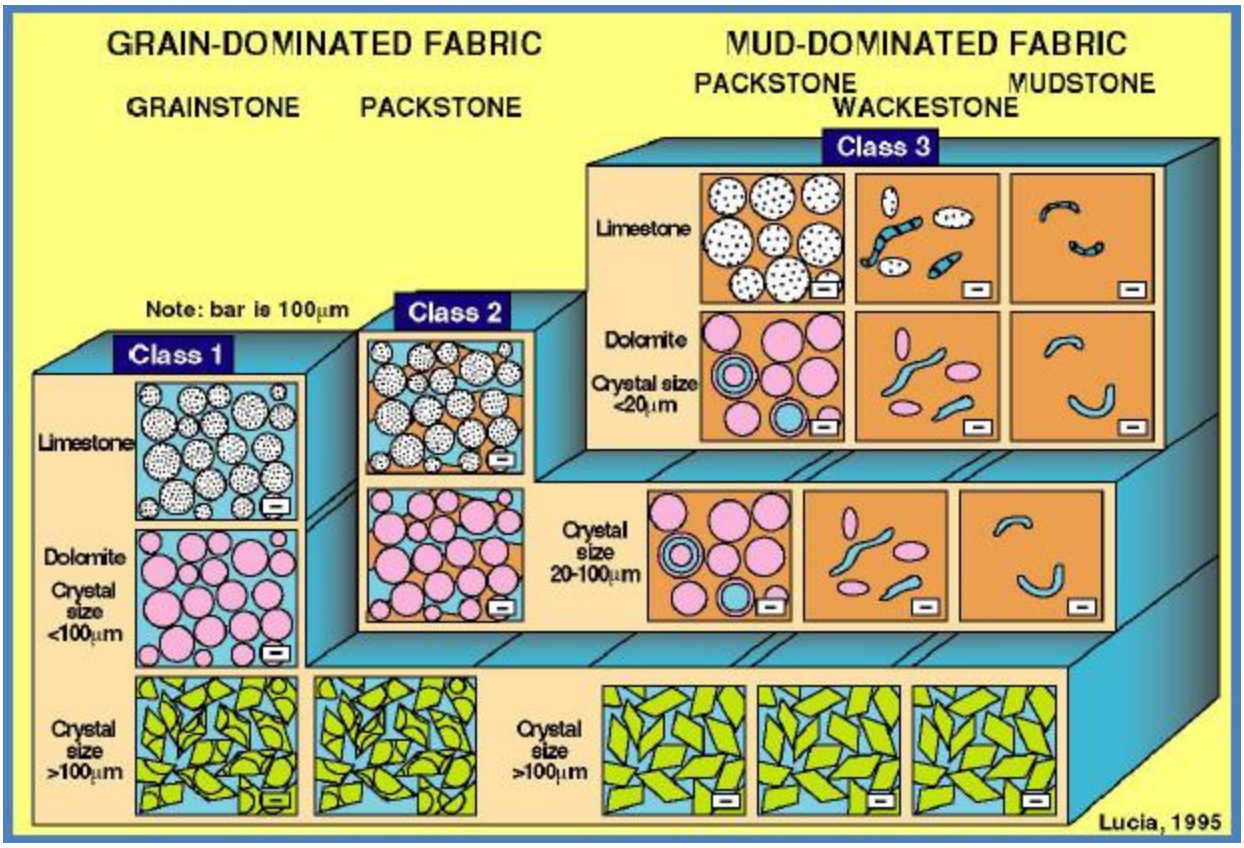

Figure 10. F. Jerry Lucia's classification of petrophysical and rock-fabric classes based on similar capillary properties and interparticle-porosity/permeability transforms (Lucia 1995).

Quantitative Measurements

Once qualitatively described, the images are quantitatively evaluated by their pore space using the image analysis software called Image-Pro Premier. The images are first cropped to avoid measuring space unoccupied by rock and to omit blue epoxy that seeped around the edges. Secondly, image editing software is used to fill in pore space that the blue epoxy failed to seep into or replace the coloration of bitumen present in many of the thin sections. Bitumen is a black or brown, viscous liquid composed of hydrocarbons that either naturally occurs in the sediment or is produced by the refinery of petroleum (Telford 1995). The images are then calibrated to 0.0069 mm per pixel to keep the resolution and measurements standardized and measurement types are inputted to include specific information on the pore space properties. These pore space

properties include area, percent area the pore occupies relative to the entire image, perimeter, length along major axis, width along minor axis, roundness, radius, average diameter, and relative size to the other voids. Next, the smart segmentation tool is utilized to distinguish between the blue epoxy in the pore space as reference objects and the rest of the rock space as background area. This creates a channel recipe based upon a range of color values given by the segmentation selections. Once the reference objects and background areas are defined, a mask is produced to ensure the program differentiates between the blue epoxy and rock space correctly (Figure 11).

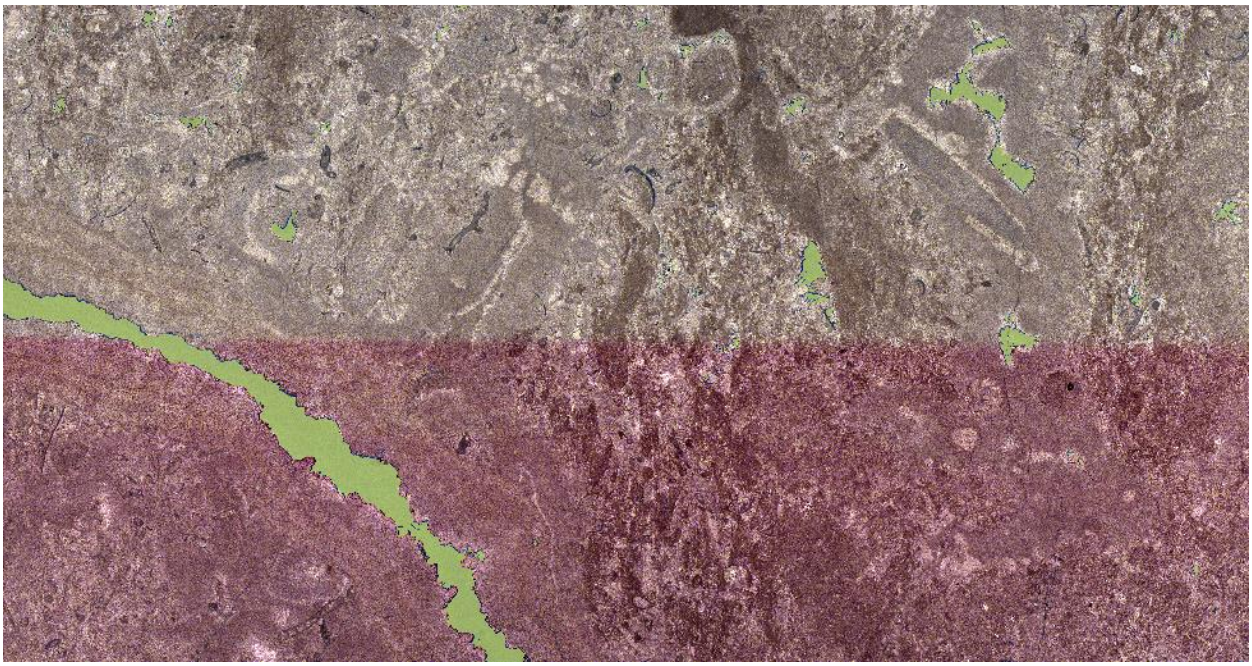

Figure 11. Mask generated of thin section I-35-9893 with blue epoxy highlighted in green.

With the blue epoxy and rock space defined properly, the count tool outlines all voids occupied by blue epoxy (Figure 12). Specific selection adjustments are made to exclude pore space on the edges of the image and manmade voids to avoid incorrect measurements. The count tool also simultaneously produces a data table on the pore space properties chosen initially.

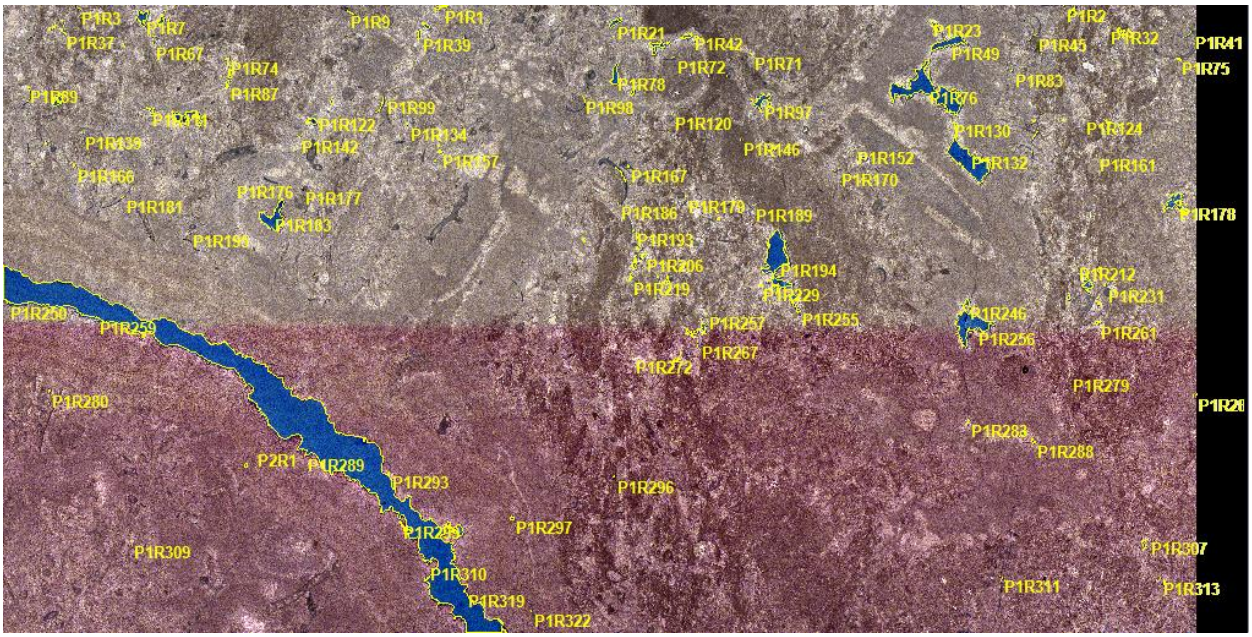

Figure 12. Utilization of the count tool on thin section I-35-9893 with blue epoxy outlined in yellow and individual pores labeled.

The main pore space properties used in this thesis are the average diameter, which determines the porosity size, and percent area the pore occupies relative to the entire image, which represents the porosity. Based upon Choquette and Pray's measurement of porosity size by average diameter per pore, the percentage of pores exhibiting microporosity (less than 1/16 mm), mesoporosity (between 1/16 mm and 4 mm), and macroporosity (greater than 4 mm) are tallied.

Well Logs

Well log data provided by Texas A&M University's Petroleum Engineering Department will be used in the future to make comparisons and correlations between the properties found using Image-Pro Premier and the actual properties present in the well logs. This will determine the accuracy of the porosity measurements from the Image-Pro Premier software and the relationships that can be made associating qualitative and quantitative data with the well logs.

Archie's Equation

An important aspect of reservoir characterization is the water saturation since its complement can be used to determine hydrocarbon or oil saturation. Many authors have already empirically related carbonate rock types with components of Archie's (1947) equation:

$$S_w = (\frac{a}{\phi^m} \times \frac{R_w}{R_t})^{\frac{1}{n}} \quad (7)$$

$$S_o = (1 - S_w) \quad (8)$$

where S_w=water saturation, S_o=oil saturation, a=tortuosity factor, ϕ=porosity, m=cementation exponent, n=saturation exponent, R_w=resistivity of formation water, and R_t=true formation resistivity of fluid and rock.

The heterogeneity of carbonates causes many of the relationships developed between *a*, *m*, and *n* to greatly vary and no set equations have been developed to describe all carbonate rocks. However, observations of vuggy and interparticle pore space display general trends with the *m* exponent as demonstrated by Lucia (1983), Focke and Munn (1987), and Borai (1987).

Borai (1987) used purely porosity values to determine the *m* exponent and used "Archie's formula with *m*=2 for medium- to high-porosity formations and the Shell formula for low-porosity formations of less than 10%." These trends may only be present in the offshore Abu Dhabi reservoir and the high heterogeneity of carbonates makes calculations of *m* values unrealistic if only based upon the degree of porosity. Other research also looks at the carbonate rock type and types of pores in understanding water saturation and permeability.

Lucia (1983) found a relationship between the *m* exponent and separate vug porosity with samples of dolomite, noting that *m* increases with percent separate vug porosity over percent total porosity as long as there are no touching vugs (Figure 13). In Lucia's research, his description of rock fabrics only applies to nonvuggy or separate vug porosity, touching-vug pore systems and porosity do not correlate in his results. He makes presumptions that touching vugs will decrease the *m* exponent, since permeability should increase with more interconnected pores, as compared to interparticle porosity.

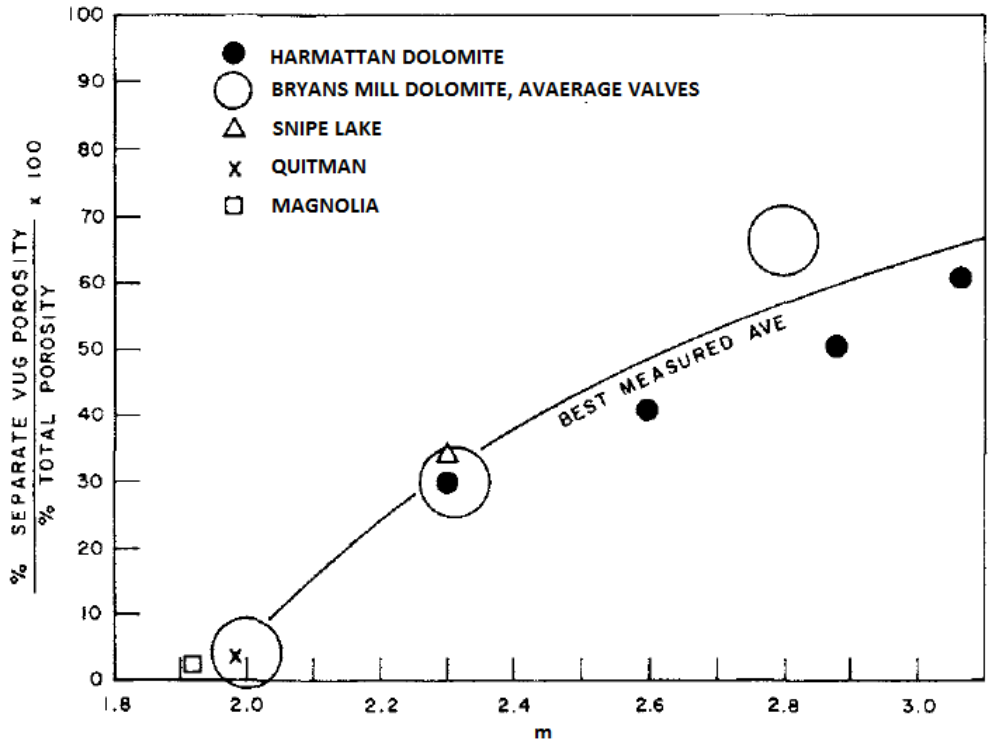

Figure 13. Measured values of *m* vs. vug porosity ratio (Lucia 1983).

Focke and Munn (1987) note that more elaborate descriptions of carbonate rock types result in a more accurate determination of *m* and therefore classified carbonate rocks from offshore reservoirs in Qatar by porosity type (Figure 14).

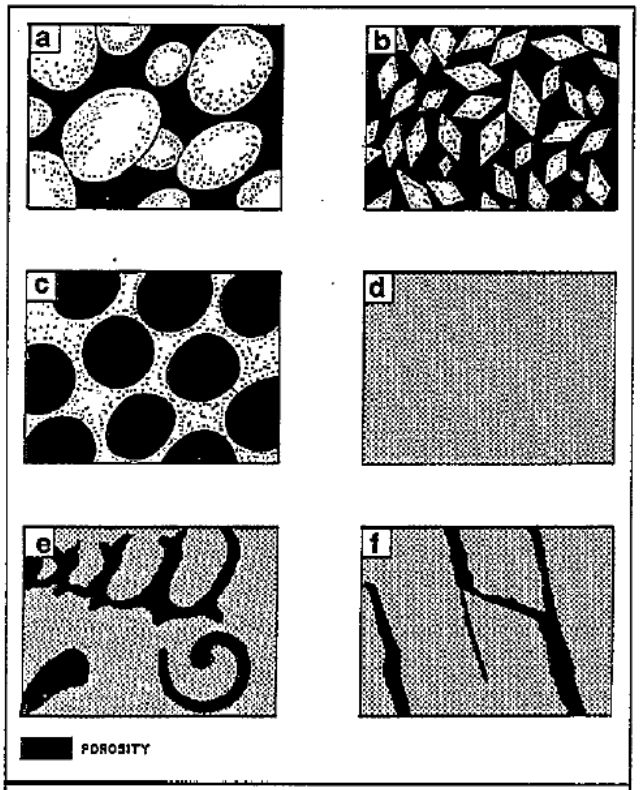

—Genetic classification of porosity type correlated with rock types: (a) intergranular (lime and dolomite grainstones, Rock Types 1 and 2; (b) intercrystalline (sucrosic dolomites, Rock Type 3); (c) moldic (moldic oolitic limestone and dolomite grainstones, Rock Types 4 and 5); (d) matrix or chalky (mudstones, chalks, Rock Type 6); (e) moldic or vuggy in addition to matrix (vuggy packstones and wackestones, Rock Type 7); and (f) fracture or fissure porosity (Rock Type 8).

Figure 14. Classification of porosity type correlated with rock types (Focke and Munn 1987).

They note that *m* can be related to grain shape with simplified models of pore geometry and the greatest *m* values are found in samples with well-developed moldic porosity. Focke and Munn discovered that rocks with interparticle pore space, Rock Types 1 through 3, showed *m* does not vary much from a value of 2.0 with increasing porosity, except at porosities less than 5%. Moldic lime grainstones, Rock Type 4, exhibit an increase in *m* with increasing porosity and *m* varies between 2.0 and 5.4. This variation exists because the pores are not touching and so the rock is less permeable, the primary porosity was filled by calcite cement, and the grains were later

dissolved to produce a wide range in the degree of cementation. Moldic dolostones, Rock Type 5, do not exhibit a distinct trend like the moldic limestones and *m* does not vary much from a value of 2.4 with increasing porosity. Mudstones and chalk, Rock Type 6, have a simple matrix porosity and *m* does not vary much from a value of 2.0 with increasing porosity. Moldic packstones and wackestones, Rock Type 7, have poorly connecting pores and *m* tends to increase above 2 with the degree of touching vugs. Fractured rocks, Rock Type 7, decrease *m* because continuous cracks through the rock promote pore connectivity and increased permeability. These rock types show how variation in porosity type and interconnectedness of pores can greatly affect the value of the cementation exponent and this causes the quantification of *m* to be difficult to simplify.

These discoveries on correlating the cementation exponent with total porosity and porosity type provide a better idea on the complexity of carbonate rock and closer approximations are obtained by first qualitatively classifying the rock. Quantitative data based upon grain shape, pore type, rock type, and degree of cementation can be used in further research on carbonates to estimate values in Archie's equation.

CHAPTER III

RESULTS

Petrographic Image Analysis

Qualitative Description

The utilization of Ahr's, Choquette and Pray's, and Lucia's three different porosity and petrophysical classifications helped compile key descriptions about the different images at various depths in the Steffan 1-35 and Steffan 2-2 cores (Appendix B).

Under Ahr's carbonate porosity classification system, the majority of images exhibit diagenetic origins of porosity in both cores and the others include both diagenetic and fracturing origins to form the Hybrid 2 class. In the Steffan 1-35 core, 69.57% of its images exhibit the Diagenetic class and 30.43% are part of the Hybrid 2 Class. In the Steffan 2-2 core, 71.43% of the images exhibit the Diagenetic class and 28.57% are part of the Hybrid 2 Class. The domination of diagenetic porosity in both cores is not surprising. All of the samples display the results of dissolution with the formation of molds and enlargement of fractures by fluid solutions; some images even show cavernous porosity. Recrystallization with the filling of void space and growth of calcite and dolomite crystals is also shown in numerous images.

Images under Choquette and Pray's carbonate porosity classification system are dominated by non-fabric selective vuggy porosity and secondly by fabric-selective moldic porosity. This demonstrates that much of the carbonates' porosity is not defined by their grains and particles and molds left behind by marine organisms still play a major role in total porosity.

Under Lucia's carbonate porosity classification system, there is a fair mix between mud- and grain-dominated fabrics, the majority of vugs are touching and fenestral, and most images appear to fall under Class 3 of the petrophysical classes. Unfortunately, Lucia's classification of petrophysical classes is supposed to be used with interparticle space without touching-vug fabrics and most of the images contain touching-vug pore space. Touching-vug pore systems and porosity do not correlate in Lucia's research, meaning the "rock fabric approach cannot be used to characterize touching-vug reservoirs" (Lucia 1995). Without values for interparticle porosity, Lucia's equations for calculating permeability and original water saturation are irrelevant in this study.

In Figure 15, Lucia and Dunham's classification of carbonates categorized the Dickinson Field thin sections from Steffan 1-35 and Steffan 2-2 into wackestones, wackestones/packstones, packstones, packstones/grainstones, and grainstones.

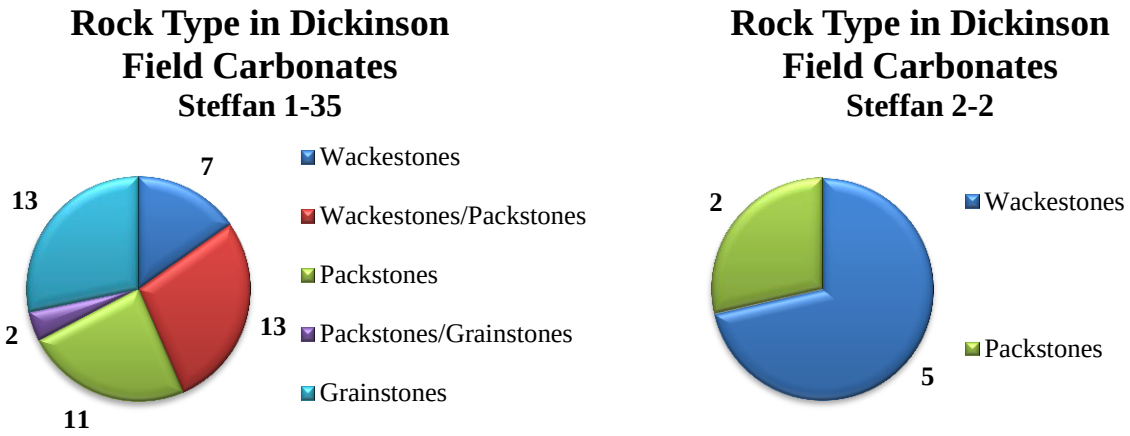

Figure 15. Carbonate rock types of thin sections from Dickinson Field.

In Figure 16, Choquette and Pray's classification further subdivided the carbonate rocks of Dickinson Field into categories defined by their porosity type, displaying how many thin sections are dominated by vuggy, moldic, channel, fracture, or interparticle porosity.

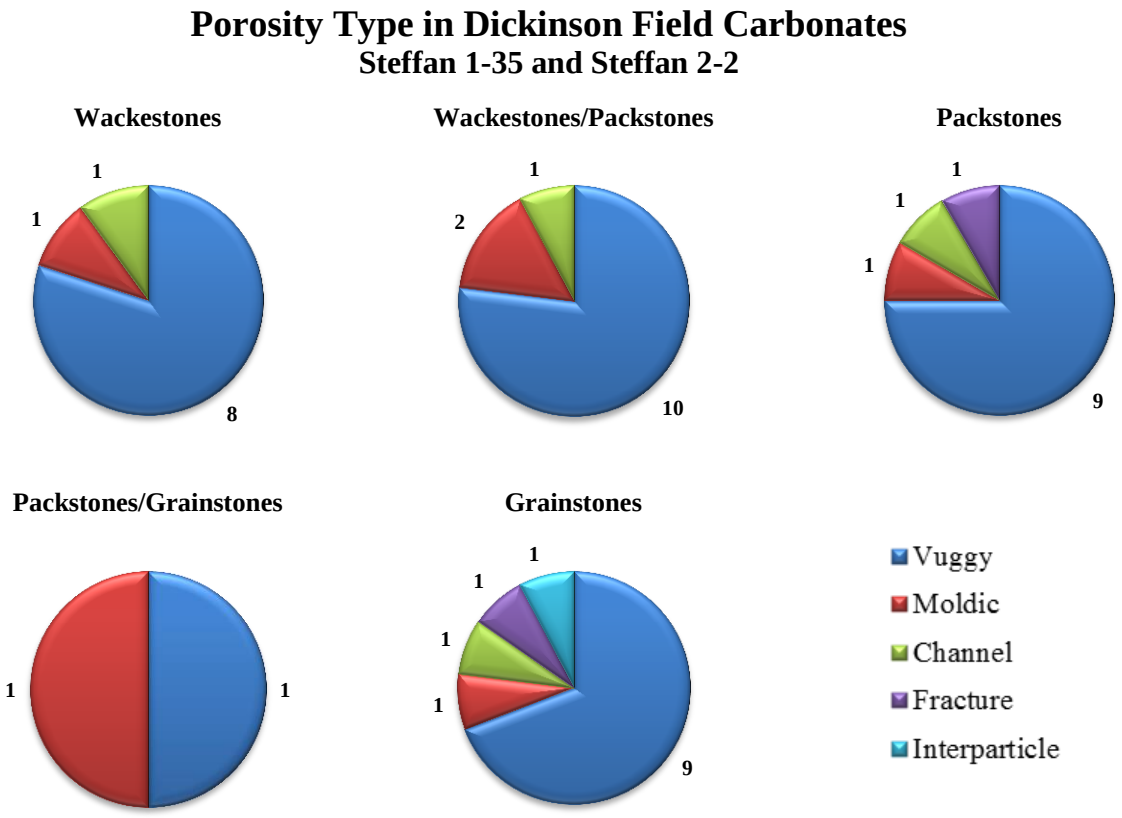

Figure 16. Carbonate porosity types in Dickinson Field.

Quantitative Measurements

Data tables produced by Image-Pro Premier calculated measurements of pore space properties, their averages, and their sums. Minor errors may have occurred from the orientation at which thin sections were originally cut, filling in void space and patches of bitumen with image editing software, and discounting pore space at the edges of images. Pore spaces may be skewed in size

when thin sections are cut, making their apparent size larger or smaller when compared to the other thin sections in the same core. Image editing software is not perfect in filling in pore space that the blue epoxy failed to seep into or replacing the coloration of bitumen since the pixel colors can vary by several tones, causing the threshold of the filling range to be difficult to determine. Pore space was discounted at the edge of images because the pores' shape and percent area could not be properly approximated. However, this also underestimates the total porosity in the image. Another issue was selecting the appropriate channel recipe when defining the void and rock space. Occasionally the software would choose a range of pixel colors unsuitable for the specification between pore and rock space, requiring extra time to properly adjust the segmentation selections.

The main pore space properties used in this thesis are the percent area the pore occupies relative to the entire image, which represents the porosity, and the average diameter, which determines the porosity size (Appendix C). In Figure 17, the total porosity of the thin sections versus depth of the cores is displayed using the percent area calculated in Image-Pro Premier. Total average porosity is approximately 2.60% for wackestones, 3.22% for wackestones/packstones, 2.55% for packstones, 2.41% for packstones/grainstones, and 4.34% for grainstones. Generally, there is an increase in total average porosity as skeletal grain content increases and when rocks become more grain-dominated in these carbonate rocks with mostly vuggy porosity. The porosity variation in the packstones may be influenced by Lucia's classification stating packstones may have either mud- or grain-dominated fabrics and many samples are on the borderline of mud- or grain-domination.

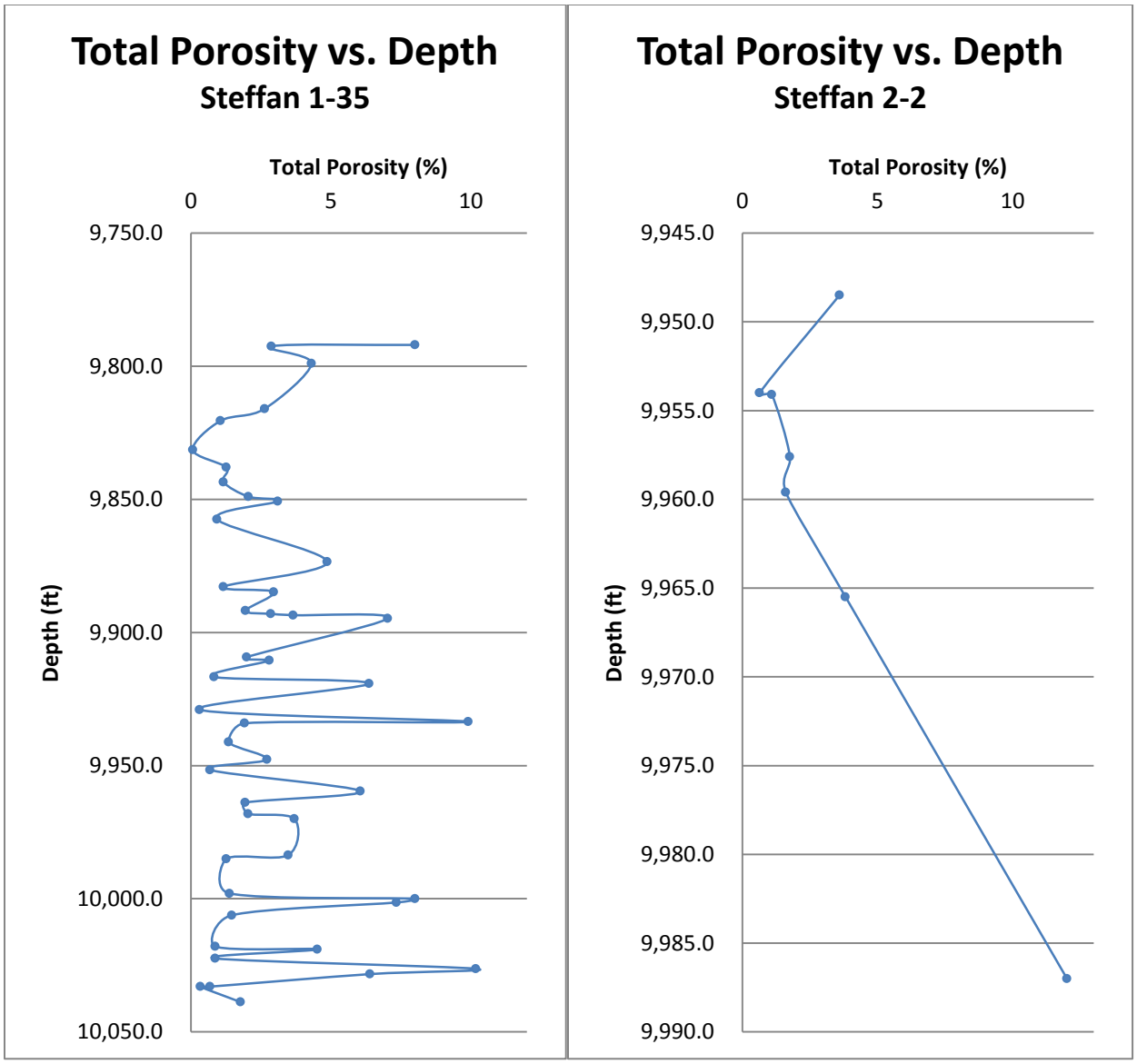

Figure 17. Total porosity calculated from Image-Pro Premier software versus depth curves in Steffan 1-35 and Steffan 2-2 cores.

In Figures 18 and 19, the percentage of pores exhibiting microporosity, mesoporosity, and macroporosity are graphed versus the depth of the cores using the average diameter per pore and Choquette and Pray's definition of porosity size.

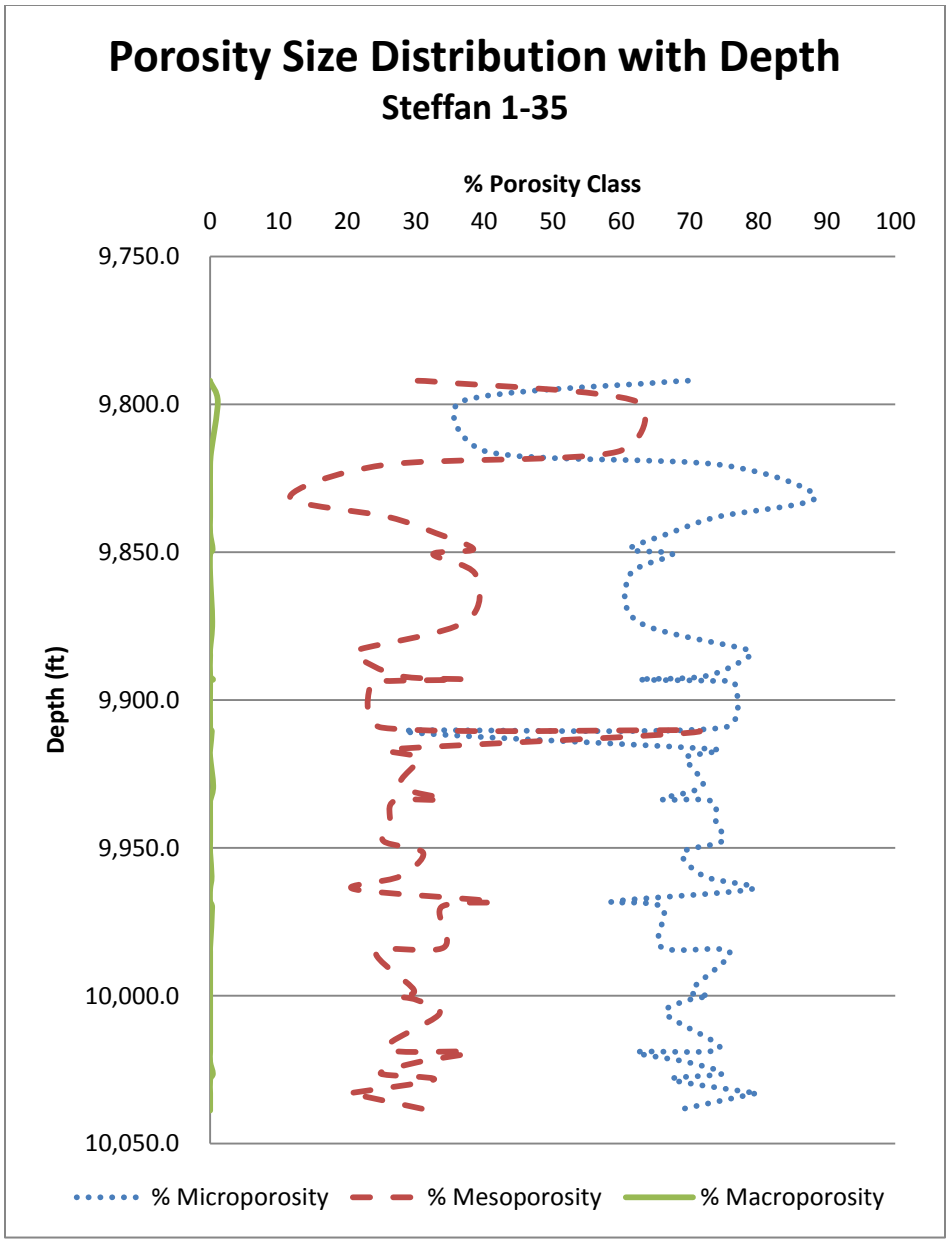

Figure 18. Porosity size distribution calculated from Image-Pro Premier software versus depth of Steffan 1-35 core.

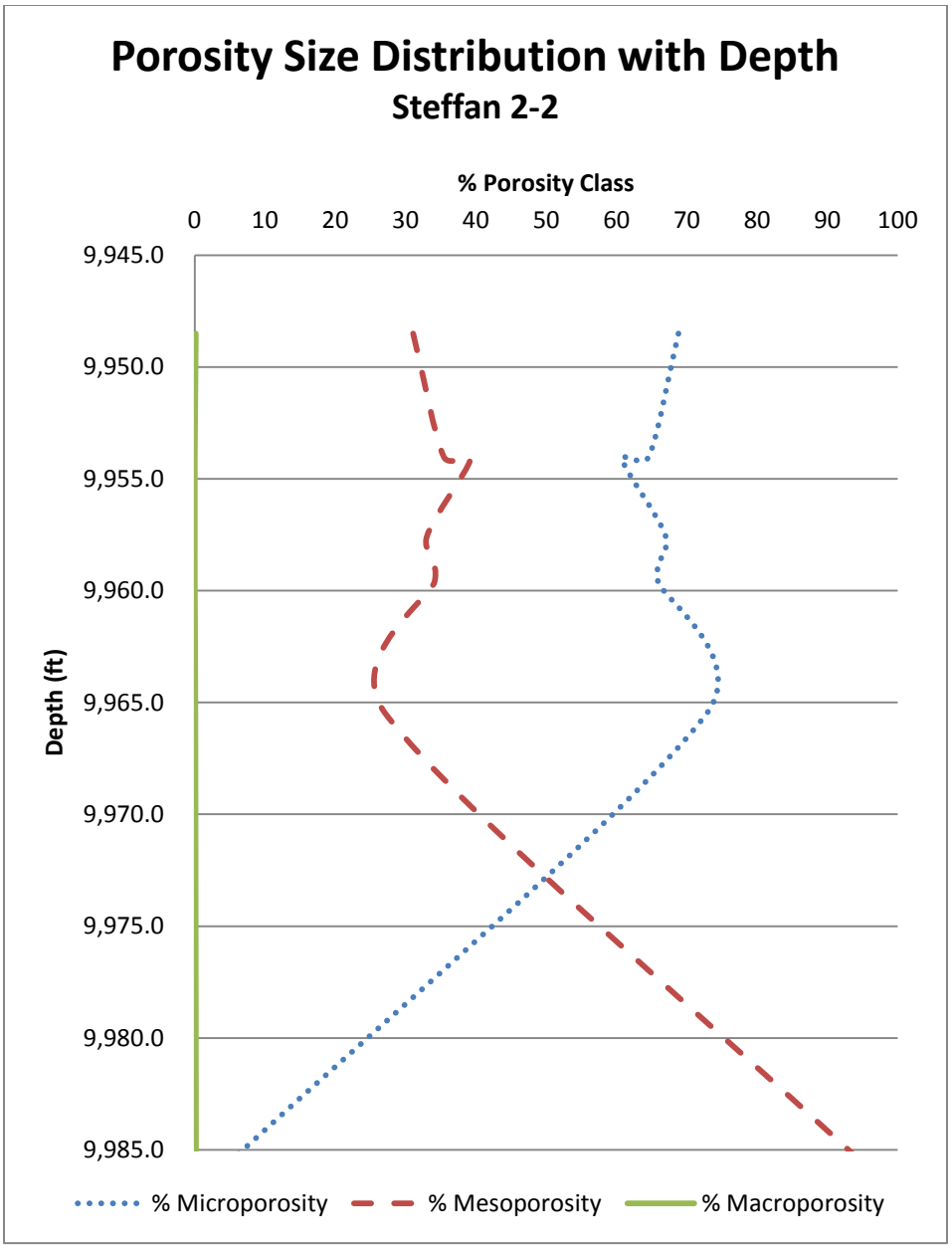

Figure 19. Porosity size distribution calculated from Image-Pro Premier software versus depth of Steffan 2-2 core.

Image-Pro Premier approximated the total porosity in the Steffan 1-35 core is on average 68.67% microporosity, 31.24% mesoporosity, and 0.09% macroporosity. The total porosity in the Steffan 2-2 core is on average 57.12% microporosity, 42.82 % mesoporosity, and 0.06% macroporosity. Since less than 1% of the total porosity in each core is macroporosity, the curves for microporosity and mesoporosity exhibit a near inverse relationship with depth. Furthermore,

Table 3 displays how all rock types are dominated by microporosity and have little to no macroporosity.

Table 3. Average porosity size distribution of total porosity in the carbonate rock types of Steffan 1-35 and Steffan 2-2.

Rock Type	Microporosity	Mesoporosity	Macroporosity
Wackestones	60.57%	33.91%	0.03%
Wackestones/Packstones	69.8%	30.11%	0.09%
Packstones	65.6%	34.31%	0.09%
Packstones/Grainstones	69.85%	30.15%	0%
Grainstones	66.6%	33.23%	0.17%

CHAPTER IV

CONCLUSION

The results show major qualitative and quantitative assessments are efficiently made using previously defined carbonate classification systems and image analysis software. The qualitative evaluations outlined by the set parameters of Ahr, Choquette and Pray, and Lucia allow for the universal description of carbonate rock and the origins of their porosity. The ease of access of the image analysis software permits the rapid collection of data on individual pore properties that can be combined into total porosity measurements and porosity size distributions.

Qualitative descriptions under Choquette and Pray's porosity classification system reinforce the complexity of carbonates since the size and development of vugs is not restricted by the fabric of the rock and molds can exhibit any size or shape from marine diversity and evolution.

Quantitative measurements are quickly produced when the correct channel recipe of segmentation is applied and they provide many useful properties on pore space. The total average porosity of both cores is approximately 3.159% and this correlates fairly well with Adam's (1999) and Burke's (1997) notes on Dickinson Field having an average of 4-5% porosity with some discrete intervals containing 10-15% porosity. Microporosity constitutes a major part of all carbonate rock types in this study and it is the most difficult pore size to manually count because of its small range in size. The software's prompt calculation of color values allows for the inclusion of all pore space sizes that could go unnoticed with physical microscope work.

Previous work using actual measurements from well logs have found empirical relationships between *m*, the cementation exponent, and porosity values in carbonates. Greater cementation generally increases the value of *m*, unless pores are isolated, and decreases water saturation values. By using quantitative measurements, like porosity size distribution, roundness, and total porosity, with the porosity types, potential models can be made comparing these properties with the *m* exponent. These models can be checked against actual well log data on water saturation to see if this quantitative data is indeed useful. For example, rocks with isolated pores can be expected to have a much higher *m* than rocks with touching pores since fluids cannot flow easily between them. Pores with a more angular than rounded shape may have a higher cementation exponent because of the irregular edges inhibiting permeability. Furthermore, the porosity size distribution is fairly consistent across all rock types, but mud- or grain- domination may affect *m* since fluids are more likely to be trapped in muddy fabrics, increasing *m*, than grain-dominated fabrics.

Overall, the image analysis software is fairly accurate in terms of approximating porosity and the various measurements the software makes can hopefully be used for future work in correlating the information with well logs and calculating components of Archie's Equation in order to easily approximate water saturation and permeability values.

REFERENCES

Adams, A. S., 1999, Depositional and Diagenetic Characteristics of Waulsortian-type Buildups in the Lodgepole Formation: Big Snowy Mountains, Montana, and Dickinson Field, North Dakota: Master's Thesis, Texas A & M University, College Station, Texas.

Ahr, W. M., 2005, Confronting the Carbonate Conundrum: Oilfield Review, v. 17, no. 1, p. 18-29.

Archie, G. E., 1947, Electrical Resistivity an Aid in Core-Analysis Interpretation: AAPG Bulletin, v. 31, no. 2, p. 350-66.

Borai, A. M., 1987, A New Correlation for the Cementation Factor in Low-Porosity Carbonates: SPE Formation Evaluation, v. 2, no. 4, p. 495-99.

Burke, R. B., 1997, Carbonate Buildup Reservoirs, Lower Mississippian Lodgepole Formation, Dickinson Field, North Dakota, USA: Proc. of CSPG-SEPM Joint Convention with the Participation of the Global Sedimentary Geology Program and the Geol. Survey of Canada: Canadian Society of Petroleum Geologists, p. 43-54.

Choquette, P. W., and L. C. Pray, 1970, Geologic Nomenclature and Classification of Porosity in Sedimentary Carbonates: The American Association of Petroleum Geologists Bulletin, v. 54, no. 2, p. 207-50.

Dunham, R. J., 1962, Classification of Carbonate Rocks According to Depositional Texture: AAPG Datapages, Memoir 1: Classification of Carbonate Rocks--A Symposium, p. 108-21.

Ehrlich, R., S.K. Kennedy, S.J. Crabtree, and R.L. Cannon, 1984, Petrographic Image Analysis, I. Analysis of Reservoir Pore Complexes: Journal of Sedimentary Petrology, v. 54, no. 4, p. 1365-378.

Focke, J. W., and D. Munn, 1987, Cementation Exponents in Middle Eastern Carbonate Reservoirs: SPE Formation Evaluation, v. 2, no. 2, p. 155-67.

Google Earth, Dickinson Field, North Dakota Map: Google, (accessed March 22, 2014).

Image-Pro Premier, Computer software, Media Cybernetics, Vers. 9.1., Roper Industries, Inc.

Johnson, M.S., 1995, Dickinson Field Lodgepole Reservoir: Significance of This Waulsortian-Type Mound to Exploration in the Williston Basin: The Mountain Geologist, v. 32, no. 3, p. 55-79.

Layman, J.M., II, 2002, Porosity Characterization Utilizing Petrographic Image Analysis Implications for Identifying and Ranking Reservoir Flow Units, Happy Spraberry Field, Garza County, Texas: Master's Thesis, Texas A & M University, College Station, Texas.

Lindquist, W.B., and A. Venkatarangan, 1999, Investigating 3D Geometry of Porous Media from High Resolution Images: Physics and Chemistry of the Earth, Part A: Solid Earth and Geodesy, v. 25, no. 7, p. 593-99.

Lucia, F. J., 1983, Petrophysical Parameters Estimated From Visual Descriptions of Carbonate Rocks: A Field Classification of Carbonate Pore Space: Journal of Petroleum Technology, v. 35, no. 3, p. 629-37.

Lucia, F. J., 1995, Rock-Fabric/Petrophysical Classification of Carbonate Pore Space for Reservoir Characterization: AAPG Bulletin, v. 79, no. 9, p. 1275-300.

Ruzyla, K., 1986, Characterization of Pore Space by Quantitative Image Analysis: SPE Formation Evaluation, v. 1, no. 4, p. 389-98.

SEPM (Society for Sedimentary Geology), Carbonate Classification - SEPM Strata: SEPM STRATA, http://www.sepmstrata.org/page.aspx?pageid=89, (accessed March 22, 2014).

Telford, Thomas, 1995, The Shell Bitumen Industrial Handbook, Chertsey: Shell Bitumen.

APPENDIX A

Condensed database information gathered from the high resolution scans of thin sections from cores of Steffan 1-35 and Steffan 2-2 in Dickinson field.

Table 4. Database information on Steffan 1-35.

Box	Name	Company/ University	Location/ Class	Field/ Site	Well	Slide	Depth (ft)	Formation	Description
6	Ahr, Wayne	Texas A&M	Stark co., ND	Dickinson	Steffan 1-35	PDP-1	9,792.0	Lodgepole	skeletal fragments, stromatactoid vugs, calcite/dolomite cement, most vugs have calcite spar lining the inside of the vug
5	Ahr, Wayne	Texas A&M	Stark co., ND	Dickinson	Steffan 1-35		9,792.5	Lodgepole	calcite/dolomite cement, skeletal fragments, intraclast
5	Ahr, Wayne	Texas A&M	Stark co., ND	Dickinson	Steffan 1-35		9,799.0	Lodgepole	calcite/dolomite cement, skeletal fragments, intraclast
5	Ahr, Wayne	Texas A&M	Stark co., ND	Dickinson	Steffan 1-35		9,816.0	Lodgepole	calcite/dolomite cement, skeletal fragments, intraclast, mud pockets, calcite sparry within the vugs
6	Ahr, Wayne	Texas A&M	Stark co., ND	Dickinson	Steffan 1-35	PDP-3	9,820.5	Lodgepole	skeletal fragments, intraclast,oolite
6	Ahr, Wayne	Texas A&M	Stark co., ND	Dickinson	Steffan 1-35	PDP-4	9,831.4	Lodgepole	skeletal fragments, intraclast, possibly calcite veins intruded
5	Ahr, Wayne	Texas A&M	Stark co., ND	Dickinson	Steffan 1-35		9,838.0	Lodgepole	calcite/dolomite cement, skeletal fragments, intraclast, radiaxial calcite cement, calcite sparry within the stromatactoid cavities, layers are inclined
5	Ahr, Wayne	Texas A&M	Stark co., ND	Dickinson	Steffan 1-35		9,843.5	Lodgepole	calcite/dolomite cement, skeletal fragments, intraclast, mud pockets, calcite sparry within the stromatactoid cavities, layers are inclined
5	Ahr, Wayne	Texas A&M	Stark co., ND	Dickinson	Steffan 1-35		9,849.0	Lodgepole	calcite/dolomite cement, mudpocket, radiaxial cement, diverse skeletal fragments, intraclast
6	Ahr, Wayne	Texas A&M	Stark co., ND	Dickinson	Steffan 1-35	PDP-5	9,850.7	Lodgepole	skeletal fragments, intraclast, oolites
5	Ahr, Wayne	Texas A&M	Stark co., ND	Dickinson	Steffan 1-35		9,857.5	Lodgepole	slightly inclined layers, mudpockets,intraclast, stromatactoid vugs, small hairline fractures healed with calcite cement
5	Ahr, Wayne	Texas A&M	Stark co., ND	Dickinson	Steffan 1-35		9,873.5	Lodgepole	diverse skeletal fragments, leaching and dissolution have enhanced pores, calcite/dolomite cement, intraclast,
6	Ahr, Wayne	Texas A&M	Stark co., ND	Dickinson	Steffan 1-35	PDP-6	9,882.8	Lodgepole	skeletal fragments, intraclast,oolites, calcite/dolomite crystals

Table 4 Continued.

Box	Name	Company/ University	Location/ Class	Field/ Site	Well	Slide	Depth (ft)	Formation	Description
6	Ahr, Wayne	Texas A&M	Stark co., ND	Dickinson	Steffan 1-35	PDP-7	9,884.8	Lodgepole	skeletal fragments, intraclast,oolites to pisolites, calcite/dolomite crystals
6	Ahr, Wayne	Texas A&M	Stark co., ND	Dickinson	Steffan 1-35	PDP-8	9,891.8	Lodgepole	skeletal fragments, intraclast,oolites to pisolites
5	Ahr, Wayne	Texas A&M	Stark co., ND	Dickinson	Steffan 1-35		9,893.0	Lodgepole	skeletal fragments, calcite/dolomite cement, intraclast, open fracture
6	Ahr, Wayne	Texas A&M	Stark co., ND	Dickinson	Steffan 1-35	PDP-9	9,893.5	Lodgepole	skeletal fragments, intraclast,oolites to pisolites
6	Ahr, Wayne	Texas A&M	Stark co., ND	Dickinson	Steffan 1-35	PDP-10	9,894.7	Lodgepole	skeletal fragments, intraclast,oolites to pisolites, calcite/dolomite crystals
6	Ahr, Wayne	Texas A&M	Stark co., ND	Dickinson	Steffan 1-35	PDP-11	9,909.3	Lodgepole	skeletal fragments, intraclast,oolites to pisolites, calcite/dolomite crystals
5	Ahr, Wayne	Texas A&M	Stark co., ND	Dickinson	Steffan 1-35		9,910.5	Lodgepole	skeletal fragments, calcite/dolomite cement, intraclast, open fracture, detrital pockets
6	Ahr, Wayne	Texas A&M	Stark co., ND	Dickinson	Steffan 1-35	PDP-12	9,916.7	Lodgepole	skeletal fragments, intraclast,oolites to pisolites, calcite/dolomite crystals
6	Ahr, Wayne	Texas A&M	Stark co., ND	Dickinson	Steffan 1-35	PDP-13	9,919.2	Lodgepole	skeletal fragments, intraclast,oolites to pisolites
5	Ahr, Wayne	Texas A&M	Stark co., ND	Dickinson	Steffan 1-35		9,929.0	Lodgepole	skeletal fragments, calcite/dolomite cement, intraclast, open fracture healed with calcite and saddle dolomite crystals, stromatactoid vugs
5	Ahr, Wayne	Texas A&M	Stark co., ND	Dickinson	Steffan 1-35		9,933.5	Lodgepole	skeletal fragments, calcite/dolomite cement, intraclast, open fracture healed with calcite and saddle dolomite crystals, stromatactoid vugs
6	Ahr, Wayne	Texas A&M	Stark co., ND	Dickinson	Steffan 1-35	PDP-14	9,934.1	Lodgepole	skeletal fragments, intraclast,oolites to pisolites, fractures
6	Ahr, Wayne	Texas A&M	Stark co., ND	Dickinson	Steffan 1-35	PDP-15	9,941.2	Lodgepole	skeletal fragments, intraclast,oolites to pisolites, fibrous and radiaxial dolomite/calcite cement
6	Ahr, Wayne	Texas A&M	Stark co., ND	Dickinson	Steffan 1-35	PDP-16	9,947.7	Lodgepole	skeletal fragments, intraclast,oolites to pisolites, fibrous and radiaxial dolomite/calcite cement
6	Ahr, Wayne	Texas A&M	Stark co., ND	Dickinson	Steffan 1-35	PDP-17	9,951.6	Lodgepole	skeletal fragments, intraclast,oolites to pisolites, fibrous and radiaxial dolomite/calcite cement
6	Ahr, Wayne	Texas A&M	Stark co., ND	Dickinson	Steffan 1-35	PDP-18	9,959.6	Lodgepole	skeletal fragments, intraclast,oolites to pisolites, fibrous and radiaxial dolomite/calcite cement
6	Ahr, Wayne	Texas A&M	Stark co., ND	Dickinson	Steffan 1-35	PDP-19	9,963.9	Lodgepole	skeletal fragments, intraclast,oolites to pisolites, calcite/dolomite cement

Table 4 Continued.

Box	Name	Company/ University	Location/ Class	Field/ Site	Well	Slide	Depth (ft)	Formation	Description
6	Ahr, Wayne	Texas A&M	Stark co., ND	Dickinson	Steffan 1-35	PDP-20	9,968.1	Lodgepole	skeletal fragments, intraclast,oolites to pisolites, calcite/dolomite cement
5	Ahr, Wayne	Texas A&M	Stark co., ND	Dickinson	Steffan 1-35		9,970.0	Lodgepole	skeletal fragments, mud pockets, calcite/dolomite cement, intraclast
6	Ahr, Wayne	Texas A&M	Stark co., ND	Dickinson	Steffan 1-35	PDP-21	9,983.6	Lodgepole	skeletal fragments, intraclast, big oolites to pisolites, calcite/dolomite cement
5	Ahr, Wayne	Texas A&M	Stark co., ND	Dickinson	Steffan 1-35		9,985.0	Lodgepole	muds are detrital, skeletal fragments, calcite/dolomite cement, intraclast
5	Ahr, Wayne	Texas A&M	Stark co., ND	Dickinson	Steffan 1-35		9,998.0	Lodgepole	skeletal fragments, mud pockets, calcite/dolomite cement, intraclast
6	Ahr, Wayne	Texas A&M	Stark co., ND	Dickinson	Steffan 1-35	PDP-22	10,000.0	Lodgepole	skeletal fragments, intraclast, big oolites to pisolites, calcite/dolomite cement
6	Ahr, Wayne	Texas A&M	Stark co., ND	Dickinson	Steffan 1-35	PDP-23	10,001.4	Lodgepole	skeletal fragments, intraclast,oolites to pisolites, calcite/dolomite cement
6	Ahr, Wayne	Texas A&M	Stark co., ND	Dickinson	Steffan 1-35	PDP-24	10,006.2	Lodgepole	skeletal fragments, intraclast,oolites to pisolites, calcite/dolomite cement
6	Ahr, Wayne	Texas A&M	Stark co., ND	Dickinson	Steffan 1-35	PDP-25	10,017.9	Lodgepole	skeletal fragments, intraclast, big oolites to pisolites, calcite/dolomite cement
5	Ahr, Wayne	Texas A&M	Stark co., ND	Dickinson	Steffan 1-35		10,019.0	Lodgepole	skeletal fragments, intraclast, calcite/dolomite cement, detrital mud pockets
7	Ahr, Wayne	Texas A&M	Stark co., ND	Dickinson	Steffan 1-35	PDP-26	10,022.4	Lodgepole	skeletal fragments, intraclast, big oolites to pisolites, calcite/dolomite cement
7	Ahr, Wayne	Texas A&M	Stark co., ND	Dickinson	Steffan 1-35	PDP-27	10,026.3	Lodgepole	diverse skeletal fragments, intraclast,oolites, calcite/dolomite cement
7	Ahr, Wayne	Texas A&M	Stark co., ND	Dickinson	Steffan 1-35	PDP-28	10,028.3	Lodgepole	skeletal fragments, intraclast,oolites , calcite/dolomite cement
7	Ahr, Wayne	Texas A&M	Stark co., ND	Dickinson	Steffan 1-35	PDP-29	10,033.0	Lodgepole	skeletal fragments, intraclast, big oolites to pisolites, calcite/dolomite cement
5	Ahr, Wayne	Texas A&M	Stark co., ND	Dickinson	Steffan 1-35		10,033.0	Lodgepole	skeletal fragments, intraclast, calcite/dolomite cement, detrital mud pockets, hydrocarbon stains and saddle dolomite crystals are scattered inside fractures
7	Ahr, Wayne	Texas A&M	Stark co., ND	Dickinson	Steffan 1-35	PDP-30	10,038.8	Lodgepole	skeletal fragments, intraclast, oolites, calcite/dolomite cement

Table 5. Database information on Steffan 2-2.

Box	Name	Company/ University	Location/ Class	Field/ Site	Well	Slide	Depth (ft)	Formation	Description
5	Ahr, Wayne	Texas A&M	Stark co., ND	Dickinson	Steffan 2-2		9,948.5	Lodgepole	fractures are healed with calcite and saddle dolomite crystals, stromatactoid vugs, calcite spar, Calcite/Dolomite cement, abundance of skeletal fragments, biomicrite matrix, intraclast
5	Ahr, Wayne	Texas A&M	Stark co., ND	Dickinson	Steffan 2-2		9,954.0	Lodgepole	fractures are healed with calcite and saddle dolomite crystals, stromatactoid vugs, calcite spar, interbedded layers of cementstone, Calcite/Dolomite cement, abundance of skeletal fragments, biomicrite matrix, intraclast
2	Adams, Andrea	Texas A&M	North Dakota	Dickinson	S2-2		9,954.1	Lodgepole	Skeletal fragments (diversity of fossils increased), calcite/dolomite cement, intraclast, biomicrite, open fracture, steeply inclined
2	Adams, Andrea	Texas A&M	North Dakota	Dickinson	S2-2		9,957.6	Lodgepole	Interbedded layers of mudstone/packstone, dolomite cement, skeletal fragments, biomicrite, intraclast, steeply bedding layers
2	Adams, Andrea	Texas A&M	North Dakota	Dickinson	S2-2		9,959.6	Lodgepole	Calcite/Dolomite cement, skeletal fragments, biomicrite, intraclast, steeply interbedded layers of mudstone
5	Ahr, Wayne	Texas A&M	Stark co., ND	Dickinson	Steffan 2-2		9,965.5	Lodgepole	fractures are healed with calcite and saddle dolomite crystals, stromatactoid vugs, calcite spar, Calcite/Dolomite cement, abundance of skeletal fragments, biomicrite matrix, intraclast
5	Ahr, Wayne	Texas A&M	Stark co., ND	Dickinson	Steffan 2-2		9,987.0	Lodgepole	skeletal fragments, calcite/dolomite cement, interbedded layers of cementstone, muds are detrital and contains fossils, stromatactoid vugs, intraclast

APPENDIX B

Qualitative image analysis data gathered from the high resolution scans of thin sections from cores of Steffan 1-35 and Steffan 2-2 in Dickinson field.

Abbreviations used in tables:

Carbonate Porosity Classification Systems:

CP = Choquette & Pray's Carbonate Porosity Classification System
L-VP = Lucia's Carbonate Porosity Classification System on Vuggy Pore Space
L-I = Lucia's Carbonate Porosity Classification System on Interparticle Pore Space
L-P = Lucia's Carbonate Porosity Classification System on Petrophysical Class
B/U = Bolded and Underlined text of characteristic dominates in image

Ahr's Carbonate Porosity Classification System:

D = Diagenetic
H2 = Hybrid 2

Choquette & Pray's Carbonate Porosity Classification System:

F = Fabric selective
NF = Non-fabric selective

Lucia's Carbonate Porosity Classification System on Vuggy Pore Space and Interparticle Pore Space:

GD = Grain-dominated fabric
MD = Mud-dominated fabric

Table 6. Qualitative image analysis data on Steffan 1-35.

Box	Well	Slide	Depth (ft)	Ahr	CP (B/U)	L-VP (B/U)	L-I	L-P
6	Steffan 1-35	PDP-1	9,792.0	D	**NF (vug)**, F (moldic)	GD; **Touching-Vug Pores (fenestral)**, Separate-Vug Pores (moldic)	GD; Packstone	2
5	Steffan 1-35		9,792.5	D	**NF (vug)**, F (moldic)	GD; **Touching-Vug Pores (fenestral)**, Separate-Vug Pores (moldic)	GD; Grainstone	1
5	Steffan 1-35		9,799.0	H2	**NF (fracture**, vug), F (moldic)	GD; **Touching-Vug Pores (solution-enlarged fractures**, fenestral), Separate-Vug Pores (moldic)	GD; Grainstone	1
5	Steffan 1-35		9,816.0	H2	**NF (vug**, fracture), F (moldic)	GD; **Touching-Vug Pores (fenestral**, solution-enlarged fractures), Separate-Vug Pores (moldic)	GD; Grainstone	1
6	Steffan 1-35	PDP-3	9,820.5	D	**NF (vug)**, F (moldic)	MD; **Touching-Vug Pores (fenestral)**, Separate-Vug Pores (moldic)	MD; Wackestone/ Packstone	3
6	Steffan 1-35	PDP-4	9,831.4	D	**NF (vug)**, F (moldic)	MD; **Touching-Vug Pores (fenestral)**, Separate-Vug Pores (moldic)	MD; Wackestone	3
5	Steffan 1-35		9,838.0	H2	**NF (vug**, fracture), F (moldic)	MD; **Touching-Vug Pores (fenestral**, solution-enlarged fractures), Separate-Vug Pores (moldic)	MD; Wackestone	3

Table 6 Continued.

Box	Well	Slide	Depth (ft)	Ahr	CP (B/U)	L-VP (B/U)	L-I	L-P
5	Steffan 1-35		9,843.5	H2	**NF (vug**, fracture)	MD; **Touching-Vug Pores (fenestral**, solution-enlarged fractures)	MD; Wackestone	3
5	Steffan 1-35		9,849.0	H2	**NF (vug**, fracture), F (moldic)	MD; **Touching-Vug Pores (fenestral**, solution-enlarged fractures), Separate-Vug Pores (moldic)	MD; Wackestone/ Packstone	3
6	Steffan 1-35	PDP-5	9,850.7	D	**NF (vug)**, F (moldic)	GD; **Touching-Vug Pores (fenestral)**, Separate-Vug Pores (moldic)	GD; Packstone	2
5	Steffan 1-35		9,857.5	H2	**NF (vug**, fracture), F (moldic)	MD; **Touching-Vug Pores (fenestral**, solution-enlarged fractures), Separate-Vug Pores (moldic)	MD; Wackestone	3
5	Steffan 1-35		9,873.5	D	**NF (vug)**, F (moldic)	GD; **Touching-Vug Pores (fenestral)**, Separate-Vug Pores (moldic)	GD; Grainstone	1
6	Steffan 1-35	PDP-6	9,882.8	D	**NF (vug)**, F (moldic)	GD; **Touching-Vug Pores (fenestral)**, Separate-Vug Pores (moldic)	GD; Grainstone	1
6	Steffan 1-35	PDP-7	9,884.8	D	**F (moldic)**, NF (vug)	GD; **Separate-Vug Pores (moldic)**, Touching-Vug Pores (fenestral)	GD; Grainstone	1

Table 6 Continued.

Box	Well	Slide	Depth (ft)	Ahr	CP (B/U)	L-VP (B/U)	L-I	L-P
6	Steffan 1-35	PDP-8	9,891.8	D	**F (moldic)**, NF (vug)	MD; **Separate-Vug Pores (moldic)**, Touching-Vug Pores (fenestral)	MD; Wackestone/ Packstone	3
5	Steffan 1-35		9,893.0	D	**NF (channel**, vug), F (moldic)	GD; **Touching-Vug Pores (cavernous**, fenestral), Separate-Vug Pores (moldic)	GD; Packstone	2
6	Steffan 1-35	PDP-9	9,893.5	D	**NF (channel**, vug), F (moldic)	MD; **Touching-Vug Pores (cavernous**, fenestral), Separate-Vug Pores (moldic)	MD; Wackestone/ Packstone	3
6	Steffan 1-35	PDP-10	9,894.7	D	**NF (vug**), F (moldic)	GD; **Touching-Vug Pores (fenestral)**, Separate-Vug Pores (moldic)	GD; Grainstone	1
6	Steffan 1-35	PDP-11	9,909.3	D	**NF (vug)**	MD; **Touching-Vug Pores (fenestral)**	MD; Packstone	3
5	Steffan 1-35		9,910.5	D	**NF (vug)**, F (moldic)	GD; **Touching-Vug Pores (fenestral)**, Separate-Vug Pores (moldic)	GD; Packstone	2
6	Steffan 1-35	PDP-12	9,916.7	D	**NF (vug)**	MD; **Touching-Vug Pores (fenestral)**	MD; Wackestone/ Packstone	3
6	Steffan 1-35	PDP-13	9,919.2	D	**NF (vug)**	MD; **Touching-Vug Pores (fenestral)**	MD; Wackestone/ Packstone	3

Table 6 Continued.

Box	Well	Slide	Depth (ft)	Ahr	CP (B/U)	L-VP (B/U)	L-I	L-P
5	Steffan 1-35		9,929.0	H2	**NF (fracture**, vug)	MD; **Touching-Vug Pores (solution-enlarged fractures**, fenestral)	MD; Packstone	3
5	Steffan 1-35		9,933.5	D	**F (moldic)**, NF (vug)	MD; **Separate-Vug Pores (moldic)**, Touching-Vug Pores (fenestral, solution-enlarged fractures),	MD; Wackestone/ Packstone	3
6	Steffan 1-35	PDP-14	9,934.1	D	**NF (vug)**, F (moldic)	MD; **Touching-Vug Pores (fenestral)**, Separate-Vug Pores (moldic)	MD; Wackestone	3
6	Steffan 1-35	PDP-15	9,941.2	D	**F (moldic**), NF (vug)	GD; **Separate-Vug Pores (moldic)**, Touching-Vug Pores (fenestral)	GD; Packstone/ Grainstone	1
6	Steffan 1-35	PDP-16	9,947.7	D	**NF (vug**, fracture), F (moldic)	MD; **Touching-Vug Pores (fenestral**, solution-enlarged fractures), Separate-Vug Pores (moldic)	MD; Wackestone	3
6	Steffan 1-35	PDP-17	9,951.6	D	**F (moldic)**, NF (vug)	MD; **Separate-Vug Pores (moldic)**, Touching-Vug Pores (fenestral)	MD; Packstone	3

Table 6 Continued.

Box	Well	Slide	Depth (ft)	Ahr	CP (B/U)	L-VP (B/U)	L-I	L-P
6	Steffan 1-35	PDP-18	9,959.6	H2	**NF (vug**, fracture, channel), F (moldic, interparticle)	MD; **Touching-Vug Pores (fenestral**, solution-enlarged fractures, cavernous), Separate-Vug Pores (moldic)	MD; Wackestone/ Packstone	3
6	Steffan 1-35	PDP-19	9,963.9	D	**NF (vug)**, F (moldic)	MD; **Touching-Vug Pores (fenestral)**, Separate-Vug Pores (moldic)	MD; Wackestone/ Packstone	3
6	Steffan 1-35	PDP-20	9,968.1	H2	**NF (vug**, fracture)	MD; **Touching-Vug Pores (fenestral**, solution-enlarged fractures)	MD; Wackestone/ Packstone	3
5	Steffan 1-35		9,970.0	D	**NF (vug)**, F (moldic)	MD; **Touching-Vug Pores (fenestral)**, Separate-Vug Pores (moldic)	MD; Wackestone/ Packstone	3
6	Steffan 1-35	PDP-21	9,983.6	H2	**NF (vug**, fracture)	GD; **Touching-Vug Pores (fenestral**, solution-enlarged fractures)	GD; Packstone/ Grainstone	1
5	Steffan 1-35		9,985.0	H2	**NF (vug**, fracture), F (moldic)	MD; **Touching-Vug Pores (fenestral**, solution-enlarged fractures), Separate-Vug Pores (moldic)	MD; Packstone	3
5	Steffan 1-35		9,998.0	D	**NF (vug)**, F (moldic)	GD; **Touching-Vug Pores (fenestral)**, Separate-Vug Pores (moldic)	GD; Packstone	2

Table 6 Continued.

Box	Well	Slide	Depth (ft)	Ahr	CP (B/U)	L-VP (B/U)	L-I	L-P
6	Steffan 1-35	PDP-22	10,000.0	D	**F (interparticle)**, NF (vug)	GD; **Touching-Vug Pores (fenestral)**	GD; Grainstone	1
6	Steffan 1-35	PDP-23	10,001.4	D	**NF (vug)**	MD; **Touching-Vug Pores (fenestral)**	MD; Packstone	3
6	Steffan 1-35	PDP-24	10,006.2	D	**NF (vug)**, F (moldic)	MD; **Touching-Vug Pores (fenestral)**, Separate-Vug Pores (moldic)	MD; Wackestone/ Packstone	3
6	Steffan 1-35	PDP-25	10,017.9	D	**NF (vug)**, F (moldic)	MD; **Touching-Vug Pores (fenestral)**, Separate-Vug Pores (moldic)	MD; Wackestone/ Packstone	3
5	Steffan 1-35		10,019.0	H2	**NF (vug**, fracture), F (moldic)	GD; **Touching-Vug Pores (fenestral**, solution-enlarged fractures), Separate-Vug Pores (moldic)	GD; Grainstone	1
7	Steffan 1-35	PDP-26	10,022.4	H2	**NF (vug**, fracture), F (moldic)	GD; **Touching-Vug Pores (fenestral**, solution-enlarged fractures), Separate-Vug Pores (moldic)	GD; Grainstone	1
7	Steffan 1-35	PDP-27	10,026.3	D	**NF (channel**, vug, fracture), F (moldic)	GD; **Touching-Vug Pores (cavernous**, fenestral, solution-enlarged fracture), Separate-Vug Pores (moldic)	GD; Grainstone	1

Table 6 Continued.

Box	Well	Slide	Depth (ft)	Ahr	CP (B/U)	L-VP (B/U)	L-I	L-P
7	Steffan 1-35	PDP-28	10,028.3	D	**NF (vug)**, F (moldic)	GD; **Touching-Vug Pores (fenestral)**, Separate-Vug Pores (moldic)	GD; Grainstone	1
7	Steffan 1-35	PDP-29	10,033.0	D	**NF (vug)**, F (moldic)	GD; **Touching-Vug Pores (fenestral)**, Separate-Vug Pores (moldic)	GD; Grainstone	1
5	Steffan 1-35		10,033.0	H2	**NF (vug**, fracture)	MD; **Touching-Vug Pores (fenestral**, solution-enlarged fractures)	MD; Wackestone	3
7	Steffan 1-35	PDP-30	10,038.8	D	**NF (vug)**	MD; **Touching-Vug Pores (fenestral)**	MD; Packstone	3

Table 7. Qualitative image analysis data on Steffan 2-2.

Box	Well	Slide	Depth (ft)	Ahr	CP (B/U)	L-VP (B/U)	L-I	L-P
5	Steffan 2-2		9,948.5	D	**NF (vug)**, F (moldic)	MD; **Touching-Vug Pores (fenestral)**, Separate-Vug Pores (moldic)	MD; Wackestone	3
5	Steffan 2-2		9,954.0	D	**NF (vug)**, F (moldic)	GD; **Touching-Vug Pores (fenestral)**, Separate-Vug Pores (moldic)	GD; Packstone	2
2	S2-2		9,954.1	D	**F (moldic**, interparticle, intraparticle), NF (vug)	MD; **Separate-Vug Pores (moldic)**, Touching-Vug Pores (fenestral)	MD; Packstone	3
2	S2-2		9,957.6	H2	**NF (fracture**, vug), F (moldic)	MD; **Touching-Vug Pores (fenestral**, solution-enlarged fractures), Separate-Vug Pores (moldic)	MD; Wackestone	3
2	S2-2		9,959.6	D	**NF (vug)**, F (moldic, intraparticle)	MD; **Touching-Vug Pores (fenestral)**, Separate-Vug Pores (moldic)	MD; Wackestone	3
5	Steffan 2-2		9,965.5	H2	**NF (channel**, vug), F (moldic)	MD; **Touching-Vug Pores (cavernous**, fenestral), Separate-Vug Pores (moldic)	MD; Wackestone	3
5	Steffan 2-2		9,987.0	D	**F (moldic)**, NF (vug)	MD; **Touching-Vug Pores (cavernous**, fenestral), Separate-Vug Pores (moldic)	MD; Wackestone	3

APPENDIX C

Quantitative image analysis data gathered from the high resolution scans of thin sections from wells 1-35 and 2-2 in Dickinson field.

Table 8. Quantitative image analysis data on Steffan 1-35.

Box	Slide	Depth (ft)	Total Average Porosity	% Microporosity	% Mesoporosity	% Macroporosity
6	PDP-1	9,792.0	8	69.72634	30.27366	0
5		9,792.5	2.870812	66.10455	33.86172	0.033727
5		9,799.0	4.304418	36.66667	62.22222	1.111111
5		9,816.0	2.627559	40.40698	59.44767	0.145349
6	PDP-3	9,820.5	1.055201	74.64286	25.35714	0
6	PDP-4	9,831.4	0.065756	88.34951	11.65049	0
5		9,838.0	1.26132	74.11765	25.88235	0
5		9,843.5	1.16039	67.10963	32.89037	0
5		9,849.0	2.052303	61.23188	38.4058	0.362319
6	PDP-5	9,850.7	3.101306	67.45407	32.54593	0
5		9,857.5	0.932339	61.27321	38.72679	0
5		9,873.5	4.866133	62.44275	37.25191	0.305344
6	PDP-6	9,882.8	1.15902	78.15315	21.84685	0
6	PDP-7	9,884.8	2.957912	78.92196	21.07804	0
6	PDP-8	9,891.8	1.948098	72.44898	27.55102	0
5		9,893.0	2.85109	62.55319	37.02128	0.425532
6	PDP-9	9,893.5	3.643973	73.02905	26.76349	0.207469
6	PDP-10	9,894.7	7.023919	76.61446	23.38554	0
6	PDP-11	9,909.3	1.984067	74.93333	25.06667	0
5		9,910.5	2.798685	28.25553	71.49877	0.2457
6	PDP-12	9,916.7	0.819166	73.85892	26.14108	0
6	PDP-13	9,919.2	6.357226	69.42405	30.57595	0
5		9,929.0	0.308259	71.875	27.67857	0.446429
5		9,933.5	9.897393	65.90185	34.03442	0.063735
6	PDP-14	9,934.1	1.917628	73.08824	26.91176	0
6	PDP-15	9,941.2	1.347337	73.82199	26.17801	0
6	PDP-16	9,947.7	2.717305	74.69388	25.30612	0
6	PDP-17	9,951.6	0.676456	68.9243	31.0757	0
6	PDP-18	9,959.6	6.053291	72.103	27.6824	0.214592

Table 8 Continued.

Box	Slide	Depth (ft)	% Total Average Porosity	% Microporosity	% Mesoporosity	% Macroporosity
6	PDP-19	9,963.9	1.93556	79.0378	20.9622	0
6	PDP-20	9,968.1	2.03573	58.82353	41.17647	0
5		9,970.0	3.693674	65.98837	33.72093	0.290698
6	PDP-21	9,983.6	3.470317	65.88235	34.11765	0
5		9,985.0	1.259864	75.77093	24.22907	0
5		9,998.0	1.376039	70.27265	29.72735	0
6	PDP-22	10,000.0	8	72.79426	27.20574	0
6	PDP-23	10,001.4	7.340072	69.86517	30.13483	0
6	PDP-24	10,006.2	1.455451	66.58098	33.41902	0
6	PDP-25	10,017.9	0.861602	74.3649	25.6351	0
5		10,019.0	4.512139	62.12625	37.65227	0.221484
7	PDP-26	10,022.4	0.863234	69.6319	30.3681	0
7	PDP-27	10,026.3	10.16782	74.7012	24.9004	0.398406
7	PDP-28	10,028.3	6.389534	67.35385	32.64615	0
7	PDP-29	10,033.0	0.679277	79.87013	20.12987	0
5		10,033.0	0.33125	79.55665	20.44335	0
7	PDP-30	10,038.8	1.768655	67.85714	32.14286	0

Table 9. Quantitative image analysis data on Steffan 2-2.

Box	Slide	Depth (ft)	% Total Average Porosity	% Microporosity	% Mesoporosity	% Macroporosity
5		9,948.5	3.596384	68.79886	31.05899	0.142146
5		9,954.0	0.644152	64.59854	35.40146	0
2		9,954.1	1.08862	60.76923	39.23077	0
2		9,957.6	1.761245	67.01449	32.98551	0
2		9,959.6	1.608385	65.89297	34.10703	0
5		9,965.5	3.818593	72.79124	27.13057	0.078186
5		9,987.0	12.01214	0	99.82729	0.172712